EA-6010-11
(Formerly FE-3800)
Dist. Category UC-90C

MATERIALS RESEARCH FOR CLEAN UTILIZATION OF COAL

QUARTERLY PROGRESS REPORT

January - March 1977

Samuel J. Schneider
Project Manager

Institute for Materials Research
National Bureau of Standards
Washington, D. C. 20234

PREPARED FOR THE UNITED STATES
ENERGY RESEARCH AND DEVELOPMENT ADMINISTRATION

Under Contract No. EA-77-A-01-6010
(Formerly E(49-1)-3800)

TABLE OF CONTENTS

		PAGE
I.	OBJECTIVE AND SCOPE OF WORK	1
II.	SUMMARY OF PROGRESS TO DATE	1
	Articles Published and Talks Presented	4
III.	DETAILED DESCRIPTION OF TECHNICAL PROGRESS	5
	1. Metal Corrosion	5
	a. Constant Strain-Rate Test	5
	b. Pre-Cracked Fracture Test	25
	2. Ceramic Deformation, Fracture and Erosion	28
	3. Chemical Degradation	48
	a. Reactions and Transformations	48
	b. Slag Characterization	58
	c. Vaporization and Chemical Transport	63
	4. Failure Avoidance Program	64

I. OBJECTIVE AND SCOPE OF WORK

Coal Gasification processes require the handling and containment of corrosive gases and liquids at high temperature and pressures, and also the handling of flowing coal particles in this environment. These severe environments cause materials failures which inhibit successful and long-time operation of the gasification systems. The project entails investigations on the wear, corrosion, chemical degradation, fracture, and deformation processes which lead to the breakdown of metals and ceramics currently being utilized in pilot plants. Studies will also be carried out on new candidate materials considered for improved performance. Special emphasis will be devoted to the development of test methods, especially short-time procedures, to evaluate the durability of materials in the gasification environments. These methods will focus on wear, impact erosion, stress corrosion, strength, deformation, slow crack growth and chemical degradation of refractories. A system has been initiated to abstract and compile all significant operating incidents from coal conversion plants. This program will provide a central information center where problems of common interest can be identified and analyzed to avoid unnecessary failures and lead to the selection of improved materials for coal conversion and utilization. Active consultation to ERDA and associated contractors will be provided as requested.

II. SUMMARY OF PROGRESS

Brief Summary

1. Metal Corrosion

a. Constant Strain-Rate Test

The slow strain rate ($1 \times 10^{-7} s^{-1}$) testing of 310, 310S, 347 SS, and Incoloy 800 at 540°C (1000°F) in H_2S saturated at room temperature with water vapor was completed. 310 SS specimens were tested in H_2 at $8.4 \times 10^{-7} s^{-1}$. One tested in H_2 at 540°C (1000°F) fractured in a brittle type manner with secondary cracking. While another 310 SS specimen tested in H_2 at 454°C (850°F) fractured in a ductile manner with no secondary cracking. Incoloy 800 specimens were tested in the same manner as 310 SS where cracking occured (low strain rates), but no loss of ductility was apparent in the Incoloy 800. All parts and equipment for testing in coal gasification environments are on hand with the exception of a distilled water reservoir and steam line heating tapes which will be delivered in two weeks.

b. Pre-Cracked Fracture Test

The modification of the elastic stress-intensity calibration for the use of the double cantilever beam specimen at elevated temperature has been completed and limits for the use of the elastic stress analysis have been established. Sample calculation for grade 310 stainless steel have been completed.

The elastic-stress-intensity calculations will be extended to the elastic-plastic stress range and applied to other materials of interest. Experimental verification of these analyses will be started.

2. Ceramic Deformation, Fracture and Erosion

Studies of creep deformation, fracture and erosion has proceeded in three major work areas: construction and assembly of a high temperature high pressure mechanical tester; accumulation of strength data on castable refractories after exposure to hydrothermal environments; and accumulation of high temperature erosion data on castable refractories. Work on the high pressure vessel is nearing completion; the vessel should be operational by this summer. Strength degradation studies after hydrothermal exposure of a high and low purity aluminum oxide refractory (calcium aluminate bonded) have been completed to 910°C; strength degradation is observed in the high purity refractory (at approximately 410°C), but not in the low purity refractory. Erosion studies as a function of particle velocity, temperature and impingement angle have been completed on a phosphate bonded refractory. A model has been developed to explain the angular dependence of the erosion rate.

3. Chemical Degradation

a. Reactions and Transformations

Construction of major components of the apparatus for x-ray examination of refractory castables under simulated gasification conditions has been completed. The system will be assembled during April 1977, and tested at high temperature. Operation will be limited to one atmosphere of pressure until the flange seals arrive. In situ x-ray diffraction measurements are expected to begin in April 1977 as proposed.

b. Slag Characterization

The main pressure vessel for viscosity determinations has been constructed and pressure tested. The viscosity of several slag compositions have been measured at ambient pressure and the predictive equation of Watt-Fereday checked against the measured values.

c. Vaporization and Chemical Transport

After several months experience with the prototype platinum tube reactor a severe gas leak developed, necessitating construction of a new reactor. Calibration tests have proceeded with this new reaction using Na_2SO_4 with the particular objective of monitoring the Na_2SO_4 vapor species which was not observed in our earlier tests. Auxiliary classical Knudsen effusion studies on Na_2SO_4 were performed to obtain equilibrium data for comparison with the reactor experimental results. Following this testing and calibration phase we plan to introduce gases such as H_2O, H_2, SO_2 and HCl into the system and determine their effect on vapor phase transport, for Na_2SO_4 and NaCl initially.

4. Failure Prevention

Continued enlargement of the Failure Prevention Information Center was carried out. Additional reports of operating experiences were received, classified, and evaluated. Programs were developed to conduct failure mode and other statistical analysis of data in the data base. Future plans are to continue to enlarge the data base and to begin issuing abstract and summary reports on failure prevention.

Articles Published and Talks Presented

G. Ugiansky, "Constant Strain Rate Testing at Elevated Temperatures," at the General Electric Research Laboratory. (Invited Lecture)

J. M. Bukowski, E. R. Fuller, Jr., C. H. Kim, and C. Robbins, "Microstructural Analysis of Hydrothermally Treated Refractory Concretes," American Concrete Institute's Symposium on Refractory Concretes, March 17, 1977, San Diego, California. (Talk)

S. M. Wiederhorn, "Refractories for Coal Gasification," University of North Carolina at Raleigh, March 17, 1977, Raleigh, North Carolina. (Talk)

F. A. Mauer, T. Negas, A. Perloff, E. N. Farabaugh and C. R. Robbins, "Analysis of MHD Electrodes and Coal Gasification Reactor Liners by Diffraction Methods," February 23, 1977, Special session on Application of Diffraction to Fossil Fuel Energy Related Materials at the American Crystallographic Association Winter Meeting, Asilomar, Pacific Grove, California. (Talk)

III. DETAILED DESCRIPTION OF TECHNICAL PROGRESS

1. Metal Corrosion

a. Constant Strain-Rate Test (G.M. Ugiansky and C.E. Johnson, 312.04)

Progress: To complete the present phase of testing before the alloys are tested in a coal gasification environment, 310, 310S, 347 stainless steel, and Incoloy 800 specimens were tested at $\approx 1 \times 10^{-7}$ s^{-1} at 540°C (1000°F) in H_2S saturated at room temperature with water vapor. The completed results are tabulated in Table 1 for the range of strain rates at which the specimens were tested.

Table 1. Properties of Alloys Tested in H_2O/H_2S or Wet H_2S at 540°C (1000°F)

Alloy	Strain Rate, s^{-1}	Elongation, %	Reduction in Area, %	Environment*
310 SS	1.3×10^{-4}	33.8	63.2	H_2O/H_2S
	7.8×10^{-5}	32.9	55.9	Wet H_2S
	5.5×10^{-5}	33.4	62.8	H_2O/H_2S
	7.2×10^{-6}	22.5	33.1	H_2O/H_2S
	3.9×10^{-6}	12.9	25.4	Wet H_2S
	3.6×10^{-6}	23.7	30.2	H_2O/H_2S
	1.1×10^{-6}	17.2	18.4	Wet H_2S
	8.4×10^{-7}	18.7	17.5	H_2O/H_2S
	1.9×10^{-7}	9.0	14.4	Wet H_2S
310 SS	1.3×10^{-4}	33.6	63.0	Wet H_2S
	1.5×10^{-5}	34.5	62.6	Wet H_2S
	7.3×10^{-6}	35.9	62.3	Wet H_2S
	8.4×10^{-7}	34.8	50.1	Wet H_2S
	1.2×10^{-7}	27.0	36.5	Wet H_2S
347 SS	1.3×10^{-4}	17.4	62.0	Wet H_2S
	3.7×10^{-5}	15.5	63.1	Wet H_2S
	7.3×10^{-6}	15.1	64.3	Wet H_2S
	8.4×10^{-7}	14.5	55.4	Wet H_2S
	8.4×10^{-7}	17.1	61.4	H_2O/H_2S
	1.2×10^{-7}	8.6	48.8	Wet H_2S
In 800	1.3×10^{-4}	32.8	68.8	Wet H_2S
	3.7×10^{-5}	33.5	65.3	Wet H_2S
	7.3×10^{-6}	34.2	55.2	Wet H_2S
	8.4×10^{-7}	32.0	49.9	Wet H_2S
	1.7×10^{-7}	35.9	55.0	Wet H_2S

*H_2O/H_2S = H_2S plus steam
Wet H_2S = H_2S saturated at room temperature with water vapor.

Because of the heavy oxide and/or sulfide scale, the reduction in area measurements on the 310S and In 800 specimen tested at $\approx 1 \times 10^{-7}$ s^{-1}

were calculated by determining the amount of metal lost on the surface of the specimen outside of the reduced area due to the formation of scale and adding this amount to the diameter of unreacted metal in the reduced area remaining after the test. The data tabulated in Table 1 are plotted in Figures 1, 2, 3, and 4 for the respective alloys. The properties of 310 SS show a considerable decrease as the strain rate is decreased (Fig. 1); whereas, the properties of lower carbon 310 S (Fig. 2) and stabilized 347 SS (Fig. 3) do not show a significant decrease except at the very slow strain rate. Even then the decrease in properties is not as significant as for the 310 SS. The properties of Incoloy 800 (Fig. 4) are only slightly affected by the decreasing strain rate.

Table 2 is a compilation of the rest of the data collected on the alloys 310, 310 S, 347 SS, and Incoloy 800 at various temperatures and environments during the preliminary testing of these alloys before testing in coal gasification environments. Here again it should be noted that the properties for the 310 SS decrease with decreasing strain rate independent of environment but at temperatures above 454°C (850°F). Some of the final tests were made on 310 SS in H_2 to further determine the effect of environment. The first 310 SS specimen was tested at 540°C (1000°F) at a strain rate of $8.4 \times 10^{-7} s^{-1}$. The H_2 was passed through hot copper turnings, two liquid N_2 traps, and P_2O_5 to trap moisture before entering the test chamber. The resulting reduction in area was 23.3%. Secondary cracking was apparent on the reduced area near the fracture as seen in Figs. 5 and 6. Fig. 7 is a higher magnification of one of the intergranular cracks seen in Fig. 6. Fig. 8 shows the intergranular cracking on the edge on the fracture surface of Fig. 5.

The second 310 specimen was first allowed to soak at 540°C (1000°F) with no load applied for 67.5 hours. This was done to sensitize the material. The specimen was then tested at 454°C (850°F) at $8.4 \times 10^{-7} s^{-1}$ in H_2. This temperature was selected since it was below any creep temperature for 310 SS but was still in the sensitizing zone (454-870°C) (958-1600°F) for 310 SS. The resulting elongation was 35% and the reduction in area was 49%. This compares to the 18% elongation and 23% reduction in area when tested at 540°C (1000°F) in the same environment and strain rate. Figs. 9 and 10 show that there is no secondary cracking. While Fig. 11 shows that the edge of the fracture surface is ductile.

The results of testing at 454°C (850°F) have given a strong indication that the cracking problem that has been seen in 310 SS is due to creep occurring in the sensitized material with fracture occurring in or near to the weaker precipitated carbide phase in the grain boundaries.

Some data has been found to partially substantiate the opinion of reduced ductility due to creep cracking in 310 SS (1).

---

(1) ASTM STP-124, 1952.

Creep-rupture elongations of 310 SS tested at 540°C (1000°F) in air were listed at 12 and 16%, much the same as our data when tested at a slow strain rate of $1 \times 10^{-6} s^{-1}$. Whereas, short time tensile tests gave elongation of 36.2% at 540°C (1000°F) which is equivalent to our data when tested at a fast strain rate ($1.3 \times 10^{-4} s^{-1}$). However, no data reported was for tests under the ultra-high vacuum needed to insure no environmental interaction. Therefore, a mechanism of failure involving environmental interaction cannot be ruled out.

Since Incoloy 800 is susceptible to sensitization, specimens were tested at temperatures where creep occurs in order to investigate the possibility of producing the same cracking problem and loss of ductility that has been seen in 310 SS. An Incoloy 800 specimen was tested at $\simeq 1 \times 10^{-6}\ s^{-1}$ at 700°C (1300°F) in H_2 with resulting elongation of 32% and reduction in area of 54.5%. The 700°C (1300°F) temperature was chosen so that the test would be well into the creep and sensitization region. Some surface cracks appeared (Fig. 12) but they seemed to be fissures opened by ductile tearing; whereas, the cracks seen on the surface of the 310 SS specimens were more distinctive with sharp and jagged edges. Fig. 13 does not show any large cracks propagating from the surface into the bulk of the specimen but does show large voids or separations within the bulk of the specimen.

Another Incoloy 800 specimen was allowed to soak at 700°C (1300°F) in H_2 for 72 hours under a no load condition and then tested at $\simeq 1 \times 10^{-6} s^{-1}$ at 540°C (1000°F) in H_2 with resulting elongation of 30% and reduction in area of 58%. No cracking and no loss of ductility was apparent as seen from Figs. 14 and 15. From the data collected, we conclude that the Incoloy 800 does not have the same susceptibility to cracking that the 310 SS has when tested under sensitizing conditions.

Fig. 16 is a flow diagram of how the coal gasification environment will be obtained. The completion of the setup for testing in coal gasification environment has been delayed- awaiting the arrival of a distilled water reservoir and steam line heating tapes which will be delivered in two weeks.

Plans: Test 310, 310S, 347, 446 stainless steels, Incoloy 800, and Inconel 671 in an oxidizing coal gasification environment containing CO, CO_2, H_2, CH_4, H_2S, and water.

Table 2. Properties of Alloys Tested At Various Temperatures in Various Environments

Alloy	Strain Rate s^{-1}	Elongation, %	Reduction in Area, %	Testing Temp. °C,(°F)	Environment
310 SS	2.0×10^{-5}	39.2	73.4	23 (73)	Wet H_2S (1)
	7.2×10^{-6}	35.9	72.6	23 (73)	Dry He
	7.2×10^{-6}	38.4	66.3	23 (73)	Dry He (2)
	4.2×10^{-6}	32.7	68.4	23 (73)	Air
	1.1×10^{-6}	35.5	75.1	23 (73)	Wet H_2S
	8.4×10^{-7}	32.9	61.2	370 (700)	Dry He
	8.4×10^{-7}	34.6	55.9	370 (700)	Wet H_2S
	8.4×10^{-7}	35.0	48.7	454 (850)	H_2 (3)
	1.3×10^{-4}	32.8	58.0	540 (1000)	Dry He
	1.3×10^{-4}	34.4	55.7	540 (1000)	Dry He (4)
	1.3×10^{-4}	36.6	60.5	540 (1000)	Dry He (5)
	7.2×10^{-6}	31.2	56.9	540 (1000)	Dry He
	1.1×10^{-6}	18.7	24.2	540 (1000)	Tank Argon
	1.1×10^{-6}	16.0	19.8	540 (1000)	Purified Argon
	8.4×10^{-7}	15.4	19.0	540 (1000)	Dry He
	8.4×10^{-7}	18.0	19.0	540 (1000)	Dry He
	8.4×10^{-7}	17.3	25.3	540 (1000)	Ultra Pure He
	8.4×10^{-7}	14.2	15.0	540 (1000)	House Vacuum, 34 Torr.
	8.4×10^{-7}	17.9	23.3	540 (1000)	H_2
	8.4×10^{-7}	11.4	14.5	815 (1500)	Air
	1.1×10^{-6}	40.6	20.8	1038 (1900)	Air
310 SS	8.4×10^{-7}	29.3	44.8	540 (1000)	House Vacuum, 34 Torr.
347 SS	8.4×10^{-7}	31.7	74.6	23 (73)	House Vacuum, 34 Torr.
	5.2×10^{-5}	16.3	64.1	540 (1000)	House Vacuum, 34 Torr.
	7.4×10^{-6}	14.5	63.7	540 (1000)	House Vacuum, 34 Torr.
	1.1×10^{-6}	14.6	57.5	540 (1000)	House Vacuum, 34 Torr.
	8.4×10^{-7}	16.1	65.9	540 (1000)	House Vacuum, 34 Torr.
In 800	8.4×10^{-7}	29.9	58.0	540 (1000)	H_2 (6)
	8.4×10^{-7}	32.3	54.4	704 (1300)	H_2

(1) Wet H_2S - H_2S saturated at room temperature with water vapor.

(2) 310 SS specimen was soaked for 72 hours at 540°C (1000°F) in dry He under a no load condition before testing in dry He at 23°C (73°F).

(3) 310 SS specimen was soaked for 67.5 hours at 540°C (1000°F) in H_2 under a no load condition before testing in H_2 at 454°C (850°F).

(4) 310 SS specimen was soaked for 72 hours at 540°C (1000°F) in dry He under a no load condition before testing in dry He at 540°C (1000°F).

(5) 310 SS specimen was soaked for 72 hours at 540°C (1000°F) in wet H_2S under a no load condition before testing in dry He at 540°C (1000°F).

(6) Incoloy 800 specimen soaked for 72 hours at 704°C (1300°F) in H_2 under a no load condition before testing in H_2 at 540°C (1000°F).

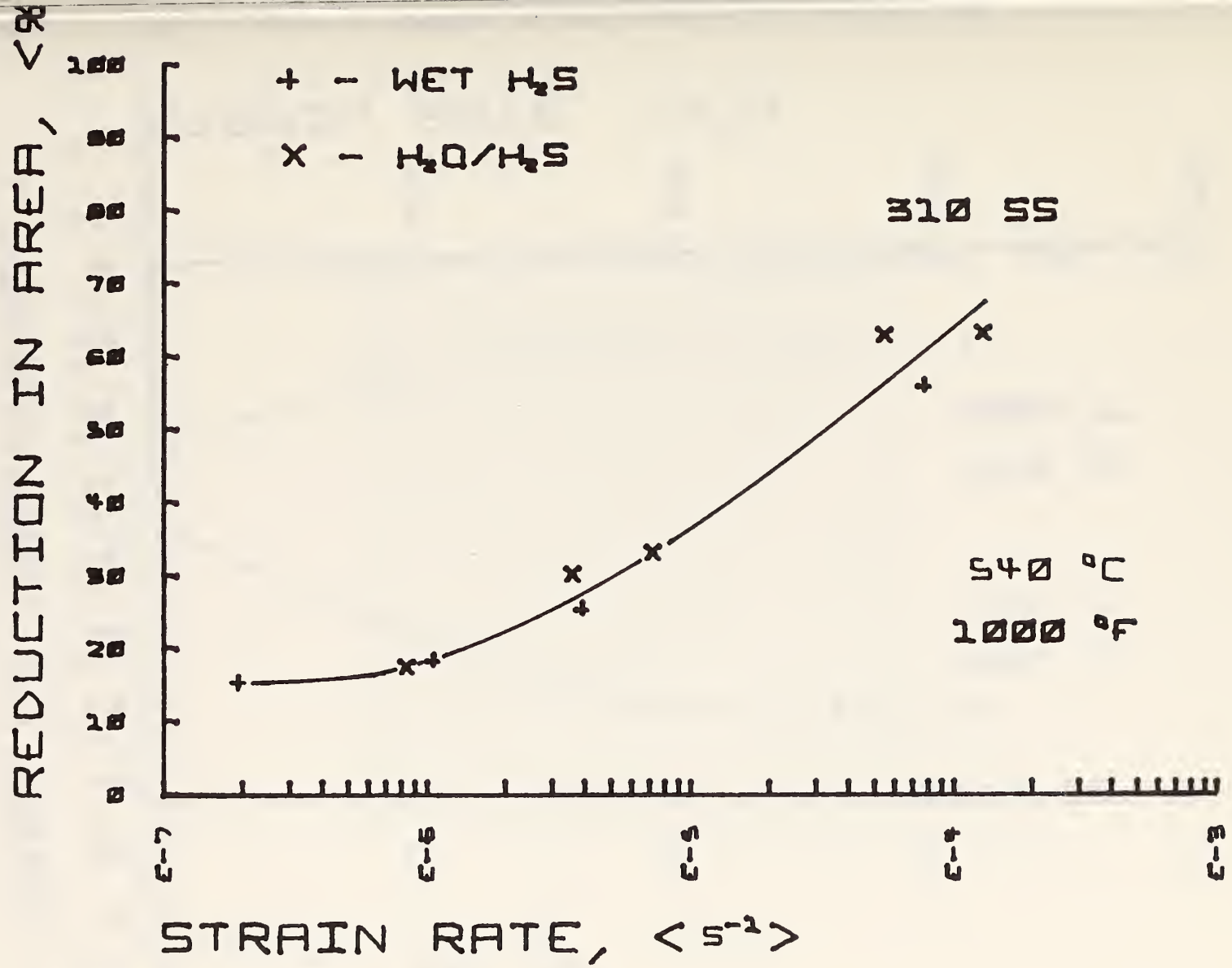

Fig. 1. Curve of reduction in area versus strain rate for 310 stainless steel. Tests conducted in saturated H_2S (wet H_2S) and in steam and H_2S (H_2O/H_2S) at 540°C (1000°F).

REDUCTION IN AREA, <%>
STRAIN RATE, <s⁻¹>
+ - WET H₂S
316SS SS
1000 °F
540 °C

Fig. 2. Curve of reduction in area versus strain rate for 310S stainless steel. Tests conducted in saturated H_2S

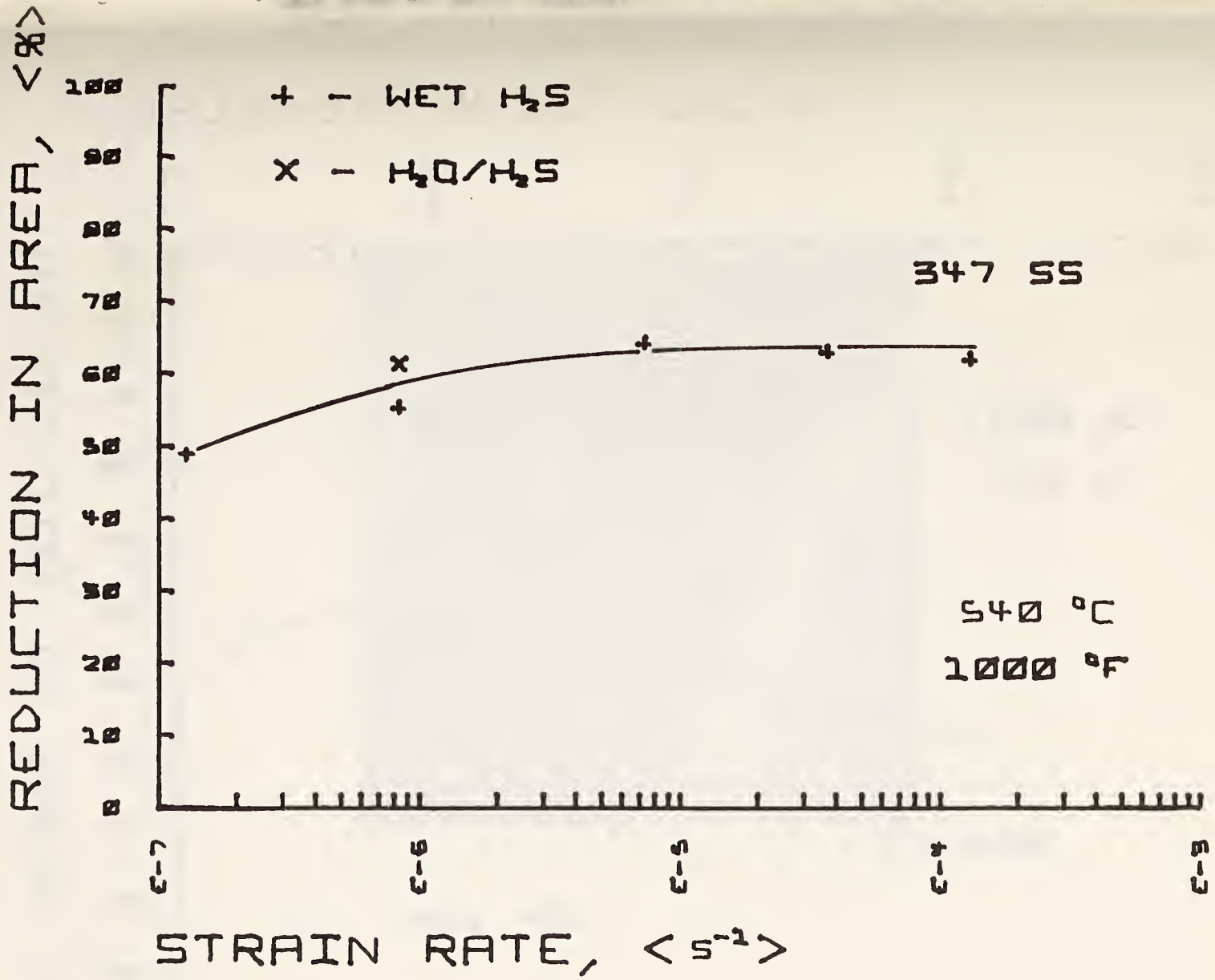

Fig. 3. Curve of reduction in area versus strain rate for 347 stainless steel. Tests conducted in saturated H_2S (wet H_2S) and in steam and H_2S (H_2O/H_2S) at 540°C (1000°F).

REDUCTION IN AREA, <%>
100
90
80
70
60
50
40
30
20
10
0
STRAIN RATE, <s⁻¹>
10⁻³
10⁻⁴
10⁻⁵
10⁻⁶
10⁻⁷
+ - WET H₂S
IN 800
540 °C
1000 °F

Fig. 5. Scanning electron micrograph of the fracture of a 310 stainless steel specimen tested at 540°C (1000°F) in H_2 at a strain rate of $8.4 \times 10^{-7} s^{-1}$. 20 X.

Fig. 6. Photomicrograph of the cross-section of the 310 stainless steel specimen in Fig. 5 tested at 540°C (1000°F) in H_2 at a strain rate of 8.4 X $10^{-7}s^{-1}$. 20 X

Fig. 7. Photomicrograph of one of the cracks penetrating into the 310 SS specimen in Fig. 6. 500 X.

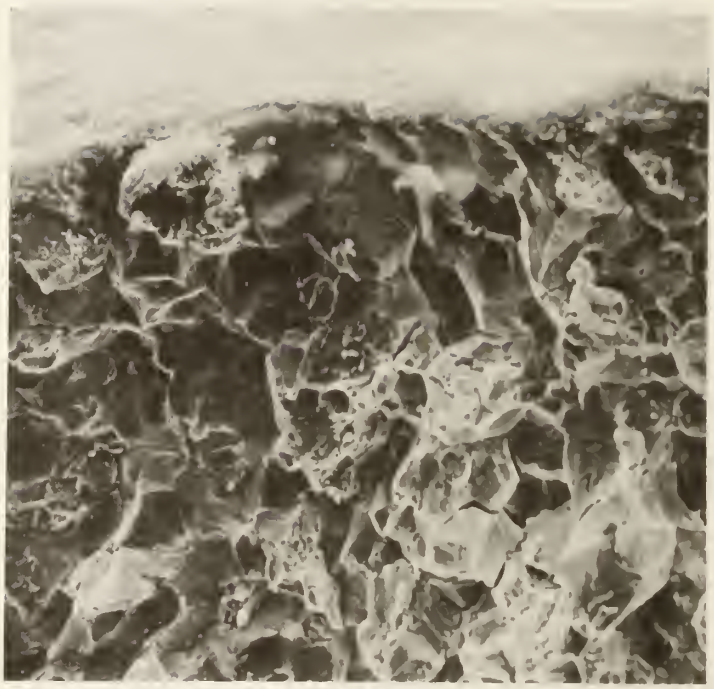

Fig. 8. Scanning electron micrograph of an area near the edge of the fracture surface of the 310 SS specimen in Fig. 5. 700 X.

Fig. 9. Scanning electron micrograph of the fracture of a 310 SS specimen tested at 454°C (850°F) in H_2 at a strain rate of 8.4 X $10^{-7}s^{-1}$. 20 X.

Fig. 10. Photomicrograph of the cross-section of the 310 SS specimen in Fig. 9. 20 X.

Fig. 11. Scanning electron micrograph of an area near the edge of the fracture surface of the 310 SS specimen in Fig. 9. 700 X.

Fig. 12. Scanning electron micrograph of the fracture of an Incoloy 800 specimen tested in H_2 at 700°C (1300°F) at a strain rate of $1 \times 10^{-6} s^{-1}$. 20 X.

Fig. 13. Photomicrograph of the cross-section of the Incoloy 800 specimen in Fig. 12. 20 X.

Fig. 14. Scanning electron micrograph of the fracture of an Incoloy 800 specimen tested in H_2 at 540°C (1000°F) at a strain rate of $1 \times 10^{-6} s^{-1}$. 20 X.

Fig. 15. Photomicrograph of the cross-section of the Incoloy 800 specimen in Fig. 14. 20 X.

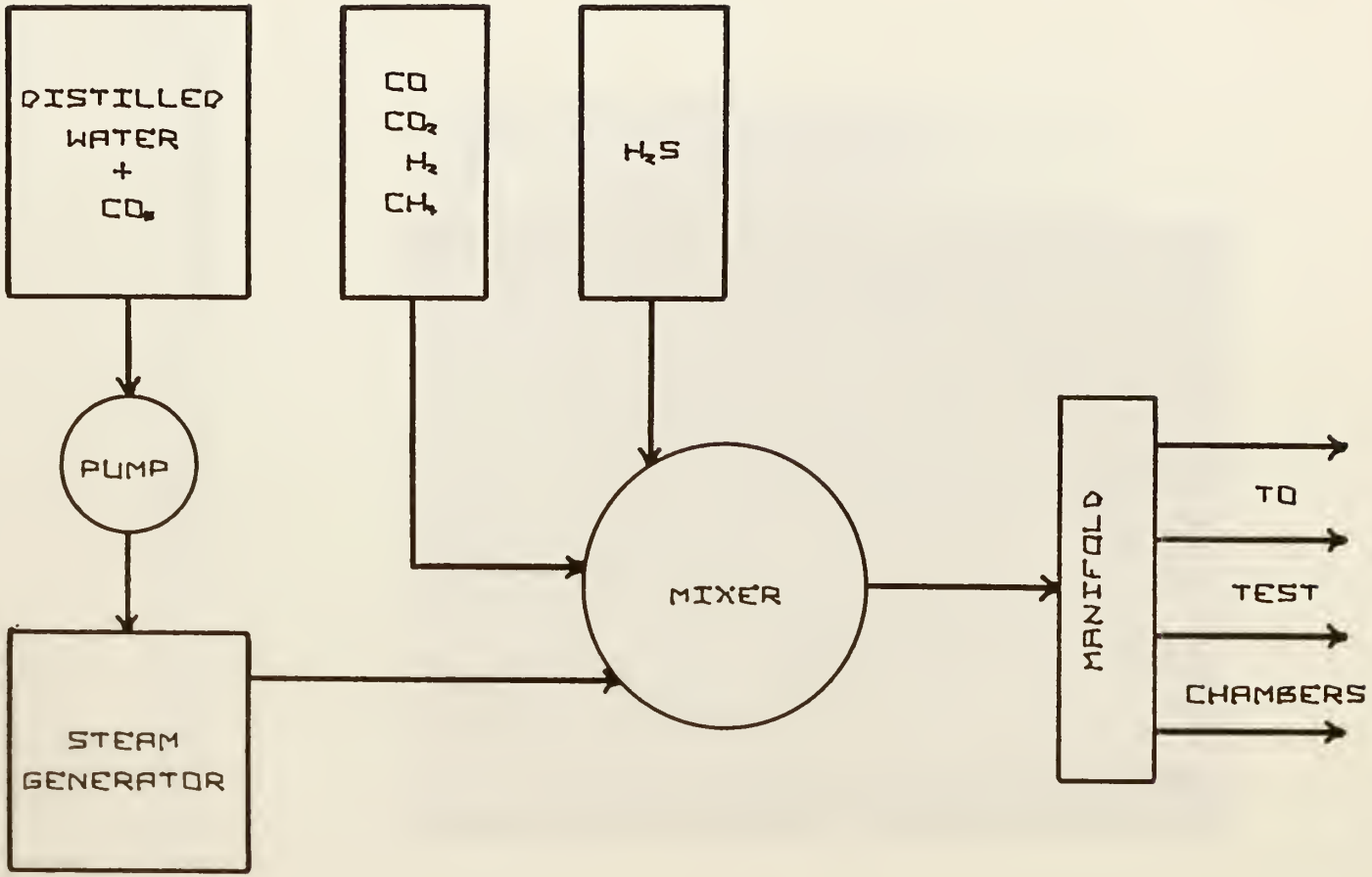

Fig. 16. Flow diagram of the generation of the coal gasification environments.

b. Pre-Cracked Fracture Test (J. H. Smith, 312.01)

Progress: The elastic stress-intensity calculation for the wedge loaded cantilever beam specimen has been modified to account for the effect of temperature on the elastic modulus and thermal expansion. This calculation equation is:

$$\frac{K_T}{K_o} = \frac{E_T}{E_o}\left[1 + \left(\frac{h_w\alpha_w - h_o\alpha_s}{h_w - h_o}\right)(T - T_o)\right]$$

where:

E_T - modulus of elasticity of specimens at test temperature, T

E_o - modulus of elasticity of specimens at loading temperature

K_T - stress-intensity at test temperature

K_o - stress-intensity at loading (reference) temperature

h_w - height of wedge at loading point

h_o - height of slot in specimen

α_w - coefficient of thermal expansion of wedge

α_s - coefficient of thermal expansion of specimen

T - test temperature

T_o - loading temperature

Sample calculations using this calibration were done for 310 stainless steel.

1. Wedge loaded DCB specimen.
2. Specimen thickness, B = 0.25 in.
3. $\alpha_w = \alpha_s$, loading wedge made of same material as specimen.
4. $h_o = 0.1 \times 10^{-2}$ m
5. $h_w = 0.8 \times 10^{-2}$ m

The results of these calculations are shown in Table A.

These results show that when the DCB specimen is loaded at room temperature and subsequently heated to elevated temperature substantial drop in the applied stress intensity at the crack tip occurs due to thermal expansion and due to the change in modulus of the material. Corrections to the stress intensity due to enlargement of the plastic zone at the crack tip were less than 5 percent up to a temperature of 600 °C.

Plans: The best available data for the strength, elastic modulus, and thermal coefficient of expansion as a function of temperature will be obtained for all materials of interest in this test program. This data will be used to calculate the effect of temperature on the elastic stress-intensity factor as a function of temperature and to determine the limit of applicability of the elastic analysis.

Suitable programs are now available to do elastic-plastic stress analyses by finite element calculation procedures. These analyses will be done for the double cantilever beam and three point bend specimens at a range of temperatures and for a range of crack lengths. These analyses must be repeated for each test material and the complete stress-strain curve must be used in the calculations at each temperature. The load versus load point displacement (compliance) curve and J_{Ic} versus load point displacement curve will be obtained from these analyses. The results of these analyses will be verified experimentally by determining the compliance of the DCB test specimen at a range of temperatures.

Table A

Effect of Temperature on Stress Intensity[1]

Temperature (°F)	$\frac{K_T}{K_o}$
0	1.00
400	0.95
800	0.88
1200	0.81
1600	0.66

2. Ceramic Deformation, Fracture and Erosion (E. R. Fuller, Jr., S. M. Wiederhorn, J. M. Bukowski, D. E. Roberts, and C. R. Robbins, 313.05)

Progress: Work on this project during the past quarter has proceeded in three major areas: Construction and assembly of a high temperature high pressure mechanical tester; accumulation of strength data on castables after exposure to hydrothermal environments; and accumulation of high temperature erosion data on castable refractories.

Pressure Vessel

The shop work on the pressure vessel is nearing completion; the remaining shop work consists of machining several minor components and of correcting any errors in design that might appear as the apparatus is tested. A schematic diagram of the equipment is shown in figure 1. As can be seen in this figure, the equipment consists of three essential parts: an environmental chamber to contain the corrosive gases; an external pressure vessel to maintain the structural integrity of the environmental chamber during operation; and a load application system to measure the fracture strength of the castable refractories at pressure and temperature. The environmental chamber and the loading fixtures that fit into the chamber are constructed of 310 stainless steel to resist the corrosive effect of the test environment. Cooler parts of the environment chamber and parts external to the chamber are made of 304 stainless steel. Load application is applied to the specimens by means of a hydraulic system that is operated by a hand pump on the control panel. To obtain near frictionless transfer of force and to maintain the atmosphere of the environmental chamber, a set of bellows (347 stainless steel) is attached to the rams that penetrate into the environment chamber. To obtain high temperatures, heating elements capable of 8 KW power are installed around the environment chamber. When completed, this equipment should be capable of operating at a temperature of 1000°C and a pressure of 1000 psi.

The high pressure vessel used to contain the environment chamber is shown in Figure 2. The vessel was constructed of a 16 inch schedule 80 steam pipe and has an overall length of approximately 65 inches. The pipe is capped by two 900 pound rated flat end flanges which contains pipe fittings for electrical and pressure lines to the test equipment (contained within the pressure vessel). The vessel was designed in accordance with the boiler codes and should be capable of 1500 psi at room temperature. Because of the massive size of the vessel, a sturdy test stand was constructed to support the vessel. The stand also provides a convenient work surface to facilitate loading of the vessel during its operation. An exhaust system was constructed as an integral part of the test stand to remove any noxious gas that might be vented into the atmosphere as a result of a leak in the vessel. To date the

pressure vessel has been assembled and hydrostatically tested to a pressure of 1500 psi for a period of 30 minutes. As there was no indication of water leakage during this period the seals on the system seemed to operate adequately.

The internal parts of the test facilities, the environment chamber and the loading ram are shown in figure 3. This part of the test equipment has an overall height of approximately 62" and so will completely fill the pressure vessel. The pressure chamber is mounted on a stainless steel stand in order to locate the chamber in a central position in the pressure vessel and to provide an adequate working distance for the loading system. The hydraulic ram and the push rods can be seen at the bottom of the figure, and the push rods that attach to the load cell can be seen at the upper part of the figure. The bellows assembly are shown in greater detail in figure 4. The interior of the vessel contains loading fixtures that will be capable of testing castable ceramic bars in three point bending. To accelerate the rate of testing the loading fixture will be capable of consecutively testing four specimens. This is accomplished by using the fixture shown in figure 5. The loading bars on the fixture are unevenly spaced so that the specimens are broken in sequence, each broken specimen falling to the bottom of the test chamber after breakage. A test fixture of similar design has been successfully used previously at NBS to study the fracture of ceramics.

Hydrothermal Exposure Tests

This part of the program is an extension of earlier work to determine the effect of coal gasification environments on the strength of castable refractories. Two types of castable ceramics were studied, Table 1: One was a high purity aluminum oxide ceramic containing approximately 94 percent alumina; the other was a calcined flint clay ceramic containing approximately 37 percent silica.

Table 1. Partial chemical compositions of castable refractories (weight percent)

Composition	A94 High Alumina castable	A56 Calcined Flint clay castable
Alumina (Al_2O_3)	94.4	55.6
Lime (CaO)	4.5	4.5
Silica (SiO_2)	0.1	37.0
Iron Oxide (Fe_2O_3)	0.1	0.8
Soda (Na_2O)	0.2	0.2

Previous exposure tests were conducted in fixed volume vessels (Morrey Bombs) which had a temperature capability of approximately 500°C. The vessels were charged with water and ceramic and then heated to various temperatures in the range 22-510°C. Strength measurements (by four-point bending) after exposure indicated a considerable contrast between the two refractories. The strength of calcined flint clay refractory (figure 6) was relatively insensitive to hydrothermal exposure over the range of temperatures studied. By contrast, severe strength degradation (figure 7) was observed in the high alumina refractory at temperatures in excess of 310°C.

Changes in strength of the castable refractories were correlated with microstructural changes in the refractories resulting from chemical interactions between the refractory and the high pressure steam. The high purity aluminum oxide refractory forms a compound, $C_4A_3H_3$ (cement density notation in which: $CaO = C$; $Al_2O_3 = A$; $H_2O = H$; $SiO_2 = S$), which has little structural integrity. The formation of the $C_4A_3H_3$ compound along with the disappearance of Boehmite (AH), which acts as a binding phase, accounts for the strength loss. By contrast, the calcined flint clay refractory forms anorthite (CAS_2) when exposed to steam. This reaction, which is similar to that occurring in earth as a result of geothermal reactions, forms a densely knit network of plate-like grains. This network remains its integrity as the refractory is cooled to low temperatures, thus accounting for the high strength of the calcined flint-clay refractory.

Because of the inability to control both temperature and pressure in a fixed volume hydrothermal apparatus, the data described above has only limited applicability to coal gasification situations. Therefore, two systems were obtained that allow the temperature and pressure to be controlled independently (figure 8). One system contains two vessels that can be used at 960°C and 1000 psi; the other system contains one vessel which can be used at 610°C and 5000 psi. These apparatus have now been used to obtain hydrothermal exposure data at temperatures and pressures that more accurately reflect conditions in coal gasifiers.

Hydrothermal experiments were conducted using two modes of operation (figure 9). In one mode of operation the vessel was heated to the final temperature before injecting steam to bring the vessel to the operating pressure. In the other mode, water was injected first so that the pressure and temperature followed the saturated vapor curve during heat-up. Once the final operating pressure was achieved, steam was vented from the vessel as required to maintain the operating pressure as the temperature was increased to the final operating temperature. This procedure was followed to evaluate the effect of heat-up procedure on the strength.

The effect of hydrothermal treatment on strength for Mode I operation is shown in figure 10. The pressure for all of these studies was 1000 psi. We note that in Mode I operation neither of the refractories studied in this project gives any indication of strength reduction as a result of exposure. In fact, a slight strength increase was registered for both refractories. Similar conclusions were reached for the calcined flint clay refractory in Mode II operation (figure 11). By contrast, the high purity aluminum oxide refractory shows strength degradation at approximately 410°C. However, as the temperature is increased to higher temperatures the strength is regained, and at 910°C the strength is the same as the specimens tested in Mode I operation. X-ray diffraction and scanning electron microscopy studies indicate that the strength loss at 410°C can be accounted for by the same reaction (the formation of the $C_4A_3H_3$ compound) as occurred in earlier studies. No firm conclusion has yet been reached on the reason for the high strengths at elevated temperatures. However, X-ray diffraction studies indicate that temperatures of 610°C and higher, the refractory dehydrates to form CA_2 and CA, and it is possible that a dehydration reaction is responsible for the increase in strength at high temperatures. Thus, it appears that for the high purity alumina refractory, there may be a danger zone ranging from about 310 to 610°C in which strength degradation can occur in the presence of high pressure water.

One of the reasons for using silica free castable refractories is to prevent the transfer of silica resulting from a water hydration reaction. In some applications this transfer results in a decrease in the efficiency of heat transfer units as a result of silica coat formation. While it is not certain that this reaction will be important in coal gasification applications, it is worth reporting that hydrothermal transfer of silica has been observed in the present set of experiments. Silica in the form of cristobalite has been found on the cool parts of the pressure vessel; the operating conditions (mode II) of the vessel at the time were 910°C, 1000 psi steam for 42 hours. The transfer had no apparent effect on the strength of the refractory.

Erosion Studies

During the past quarter studies to investigate the effect of angle of impingement on the erosion rate were continued. Measurements were conducted on a phosphate bonded refractory using 100 mesh silicon carbide particles. The results of this study, figure 12 can be compared with a study conducted earlier on a high purity castable alumina, figure 13. The erosion rate measured in these figures give the weight loss from the refractory, divided by the weight of particle hitting the specimen. The particle velocity for these studies was kept constant at a value of 72 m/s for the 25 °C data and a value of 90-95 m/s for 1000 °C data. Generally, the appearance of the two sets of curves is similar suggesting that the mechanism of erosion is the same for both types of refractories. We note that for impingement angles ranging from 30° to 90°, there is only a small change in erosion rate. At 15° impingement the erosion rate appears to drop more rapidly for 3 of the 4 graphs shown in these figures (room temperature erosion of the high alumina refractory shows only a slight decrease in rate of 15°).

The rate of erosion of these castable refractories is controlled mainly by the rate of wear of the cement phase holding the agregate particles together. Thus, as erosion proceeds channels develop in the refractories and when the channeling is sufficiently developed, the aggregate particles fall from the refractory surface. The formation of channels accounts for the relative insensitivity of these refractories to angle of impingement, because within each channel impact occurs normal to the cement surface. However, when the angle of impingement decreased below a critical value, shadowing of the surface by the exposed aggregate particles will occur resulting in a net decrease in the erosion rate. For three of the four examples given in figure 12 and 13 shadowing appears to become effective at angles ranging from between 15° and 30°. We have no ready explanation for the behavior of the fourth example. However, it should be noted that channels did not form on this refractory, suggesting that the erosion resistance of the cement phase was nearly as great as the aggregate phase.

Erosion measurements have also been made on castable refractories that have been exposed to hydrothermal environments. This study is an extension of an earlier one, in which the erosion rate was found to be related to the strength of the castable after exposure to steam. For each set of specimens prepared for strength measurements, a second set was prepared for erosion studies. Both sets were made from the same batch and given the same hydrothermal exposure. Erosion studies to date were conducted only on specimens that exhibited high strength after exposure. These specimens also were observed to have a relatively high resistance to erosion in agreement with earlier studies on the same refractory. A summary of the data collected on the specimens studied is given in table 2.

Table II. Erosive Wear of Hydrothermally Treated Castable Refractories

Hydrothermal Temperature (°C)	Strength (MPa)	Erosion Rate (mg/gm of abrasive)
Calcined Flint Clay		
untreated	10.1	20.3
110	13.9	13.3
310	10.9	13.3
410	15.2	16.0
610	15.5	14.0
710	15.2	16.0
910	14.8	13.6
High Purity Alumina Refractory		
untreated	17.4	18.2
110	23.4	9.6
310	24.1	14.6
410	27.1	15.2
610	24.8	9.2
710	25.1	10.2
910	28.0	11.6

Plans: Construction of the high pressure vessel for mechanical testing in simulated gasification environments will be continued. First the heating elements will be attached to the equipment and the heat zone will be characterized as a function of temperature and pressure. Then the pressure regulating system will be installed and checked to determine its characteristics. Once the heating and pressure system have been demonstrated, the load system will be installed and the operation of the hydraulic ram, bellows and load cell will be checked using castable refractory specimens at ambient, high and low temperatures but at pressure. Finally the water injector will be installed and the system will be operated with steam in the enviornmental chamber. When this check-out scheme has been completed, the system will be operational and systematic studies on castable refractories will be started. The system is expected to be operational at the end of the coming quarter.

Exposure studies will continue on both the high purity alumina and the calcined flint clay castable refractories. The environments to be used will be H_2O-CO_2 mixtures and H_2O-CO-CO_2-CH_4-H_2 mixtures. With the exception of H_2S and NH_3, the latter mixture will fully simulate the coal gasification environment. As in the previous studies, a range of temperature, pressure and exposure time will be investigated. The dependence of strength on heat-up procedure will also be studied. X-ray diffraction and scanning electron microscopy will be used to identify important phase changes that occur during exposure.

In the erosion studies, work on the effect of temperatures and impingement angle on the wear rate will be completed. A study will then be initiated to determine the effect of particle size and particle type on the erosion rate. The particles to be used in these studies will include silicon carbide, sand and glass spheres ranging in size from approximately 70 micrometers to approximately 1 millimeter. The size range and the types of particles should approximate the erosion characteristics of particles found in gasifiers. Erosion studies will also be conducted on castable refractories that have been exposed to hydrothermal environments.

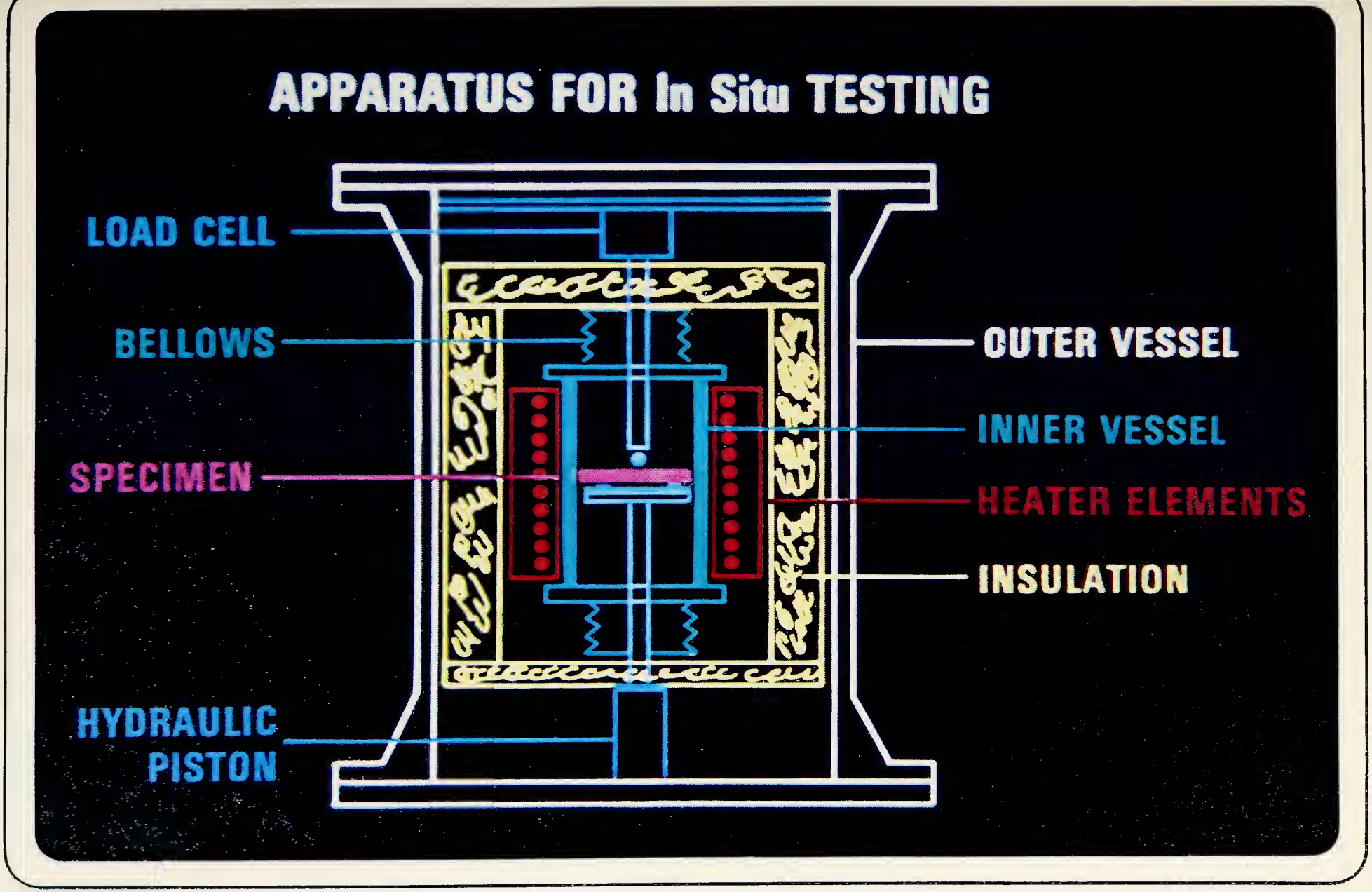

Figure 1. Schematic diagram of high pressure vessel for in situ testing.

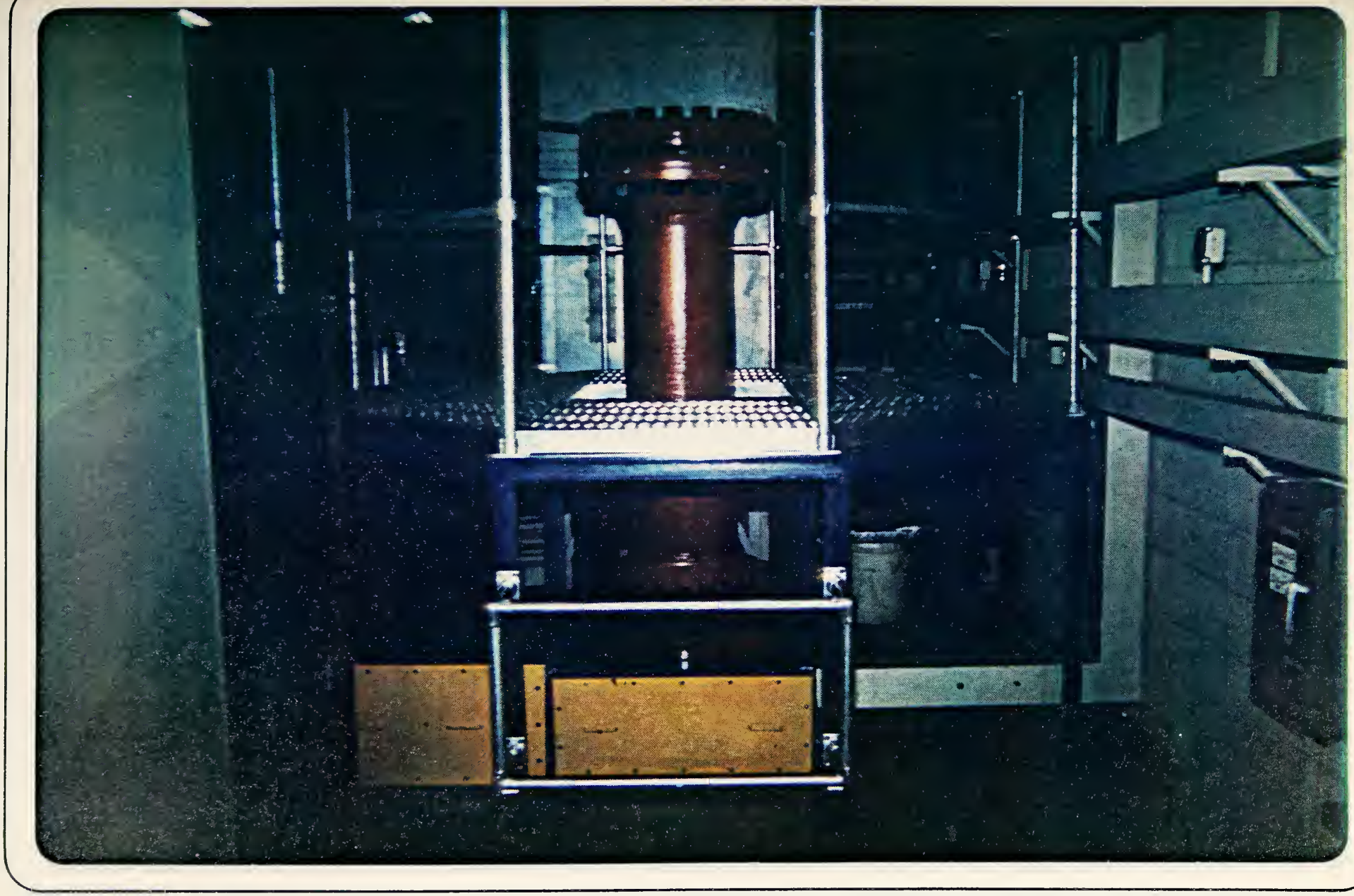

Figure 2. External view of high pressure vessel and associated attachments.

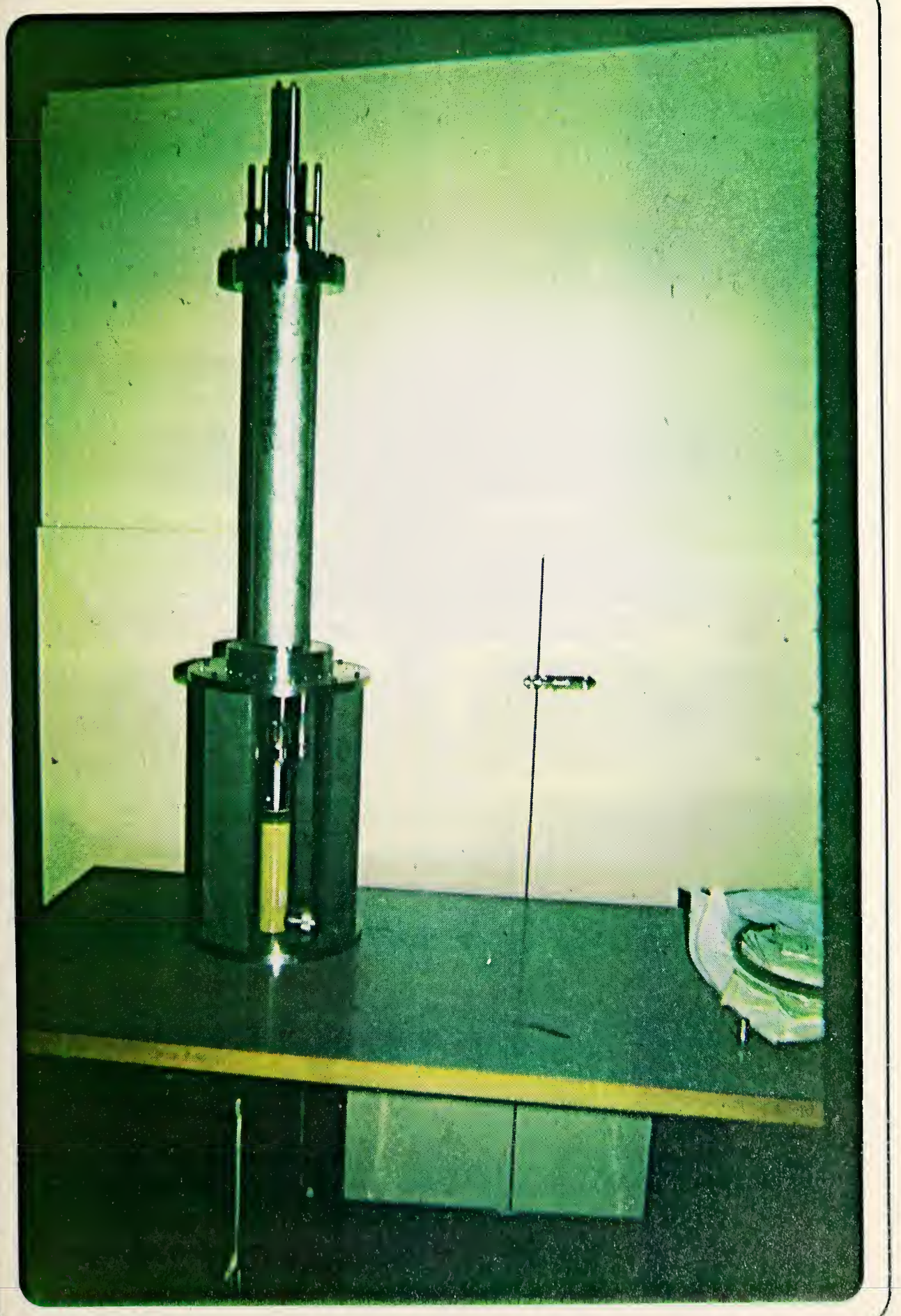

Figure 3. Environmental chamber assembly.

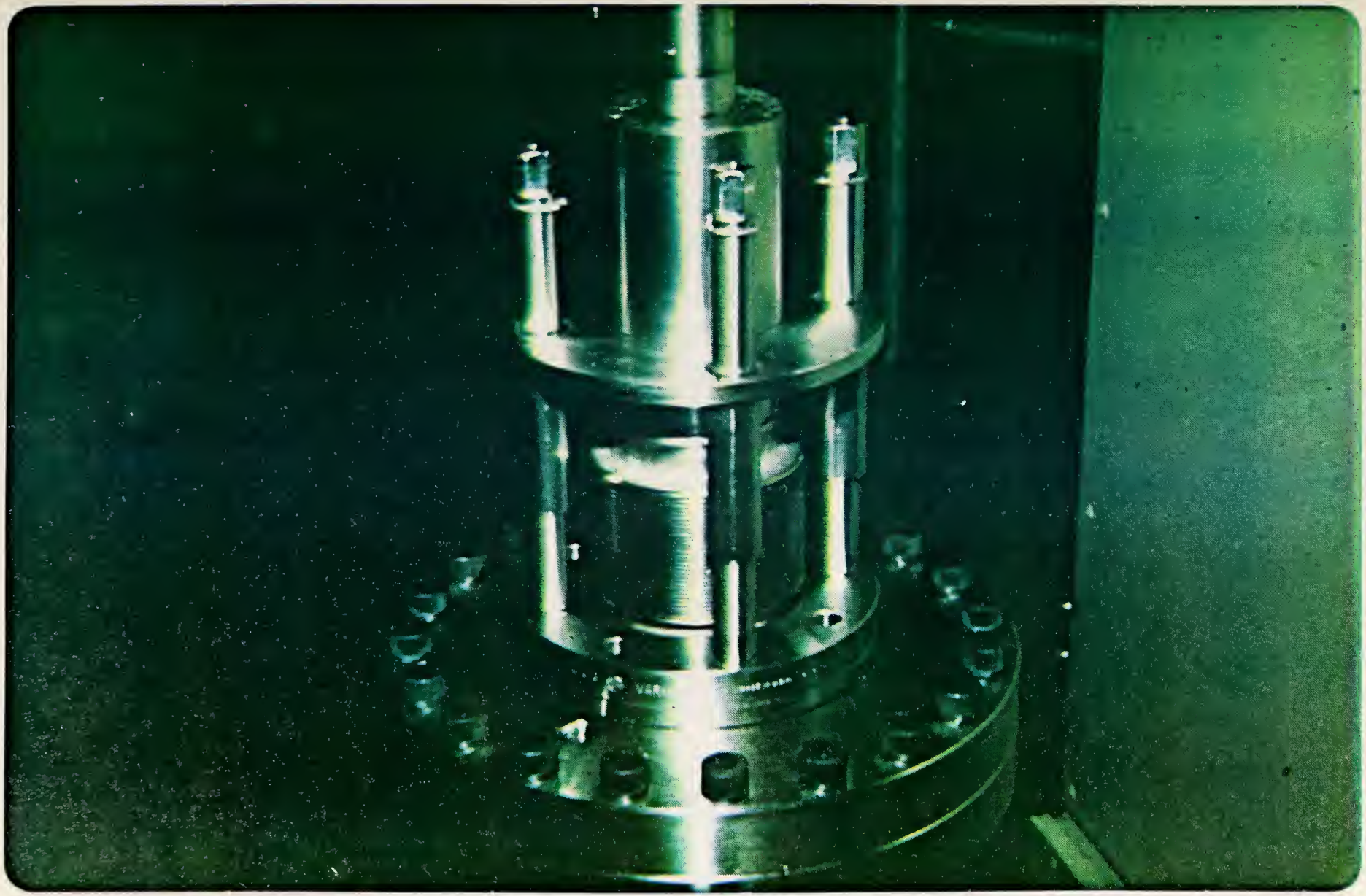

Figure 4. Bellows assembly used to isolate the environmental chamber from the pressure vessel.

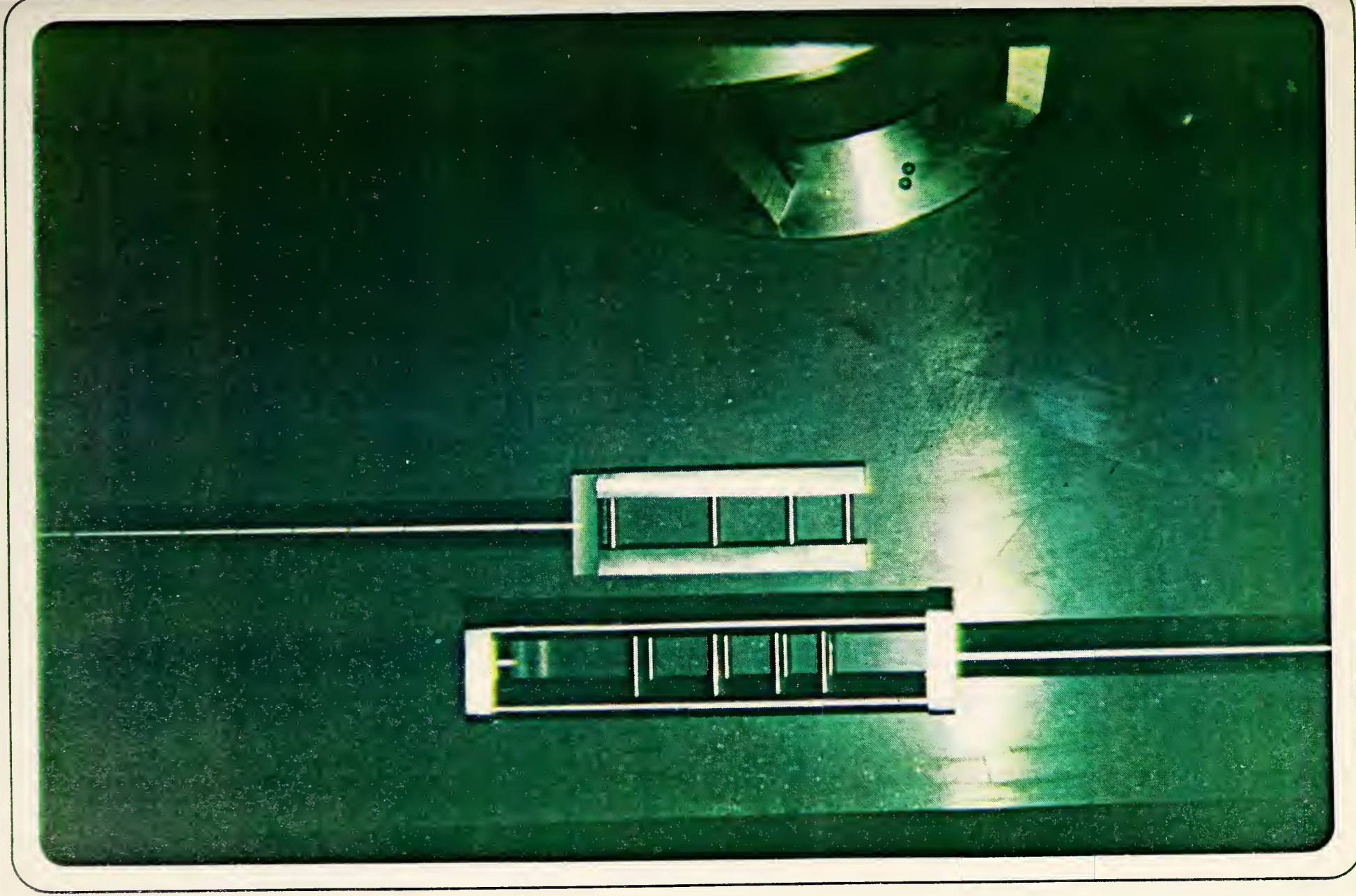

Figure 5. Loading fixture for three-point bend tests.

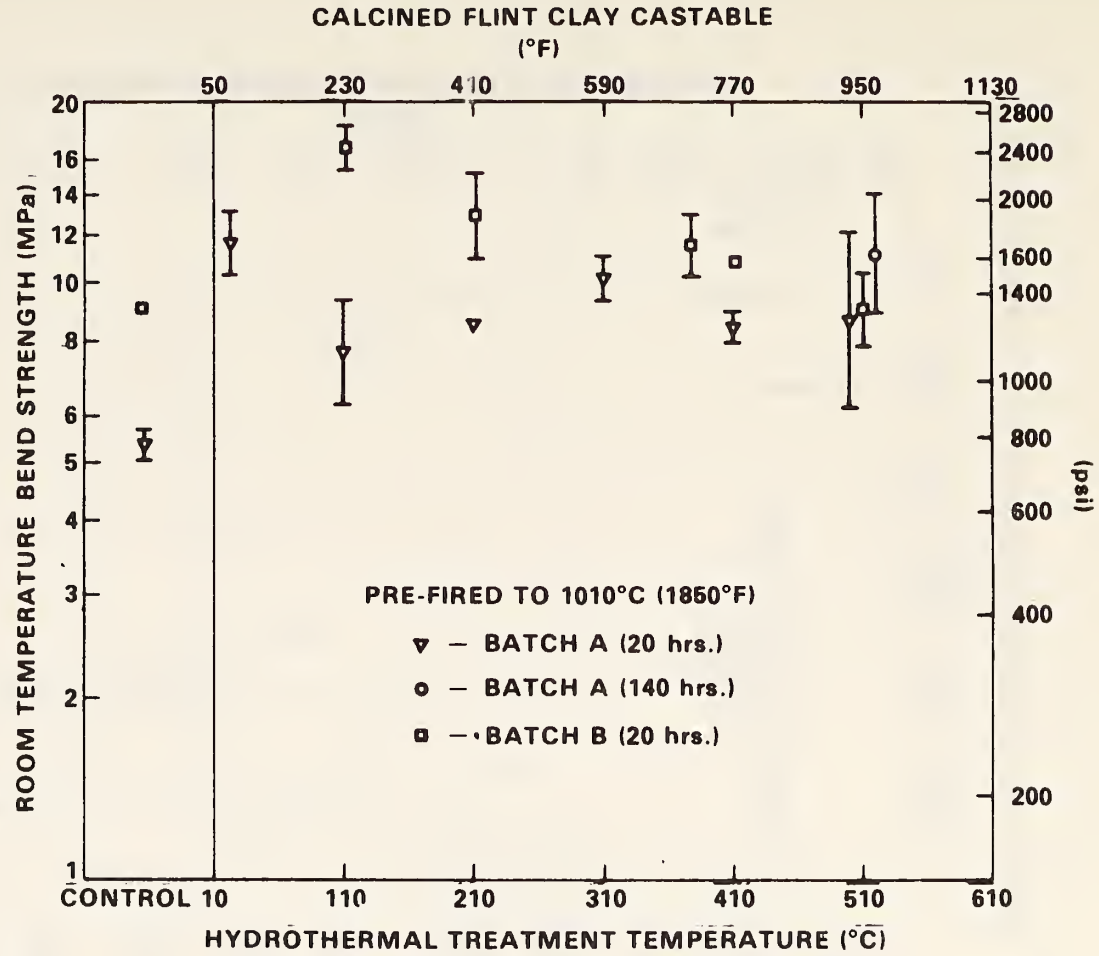

Figure 6. Bend strength of calcined flint clay castable refractory as a function of hydrothermal treatment.

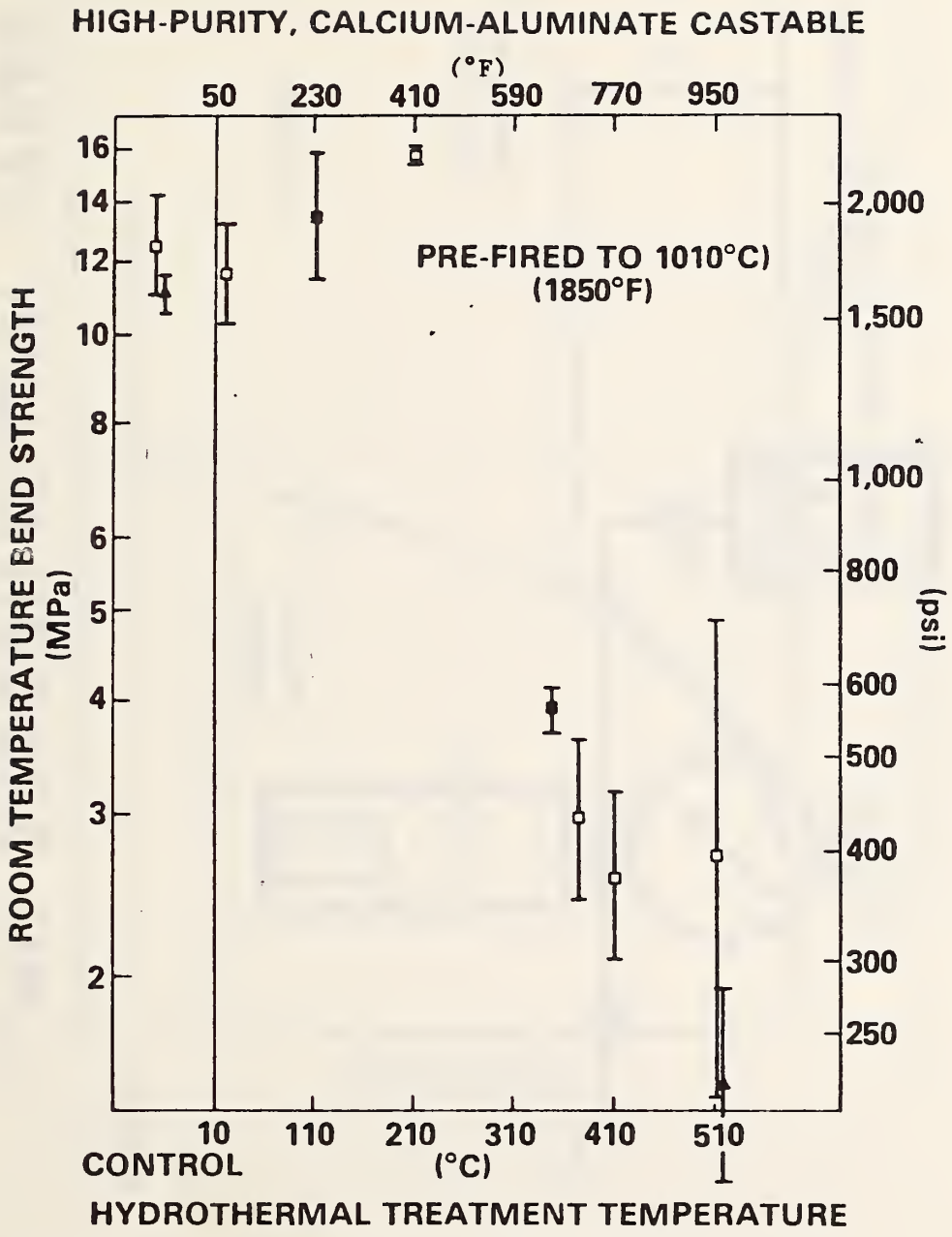

Figure 7. Bend strength of high alumina castable refractory as a function of hydrothermal treatment.

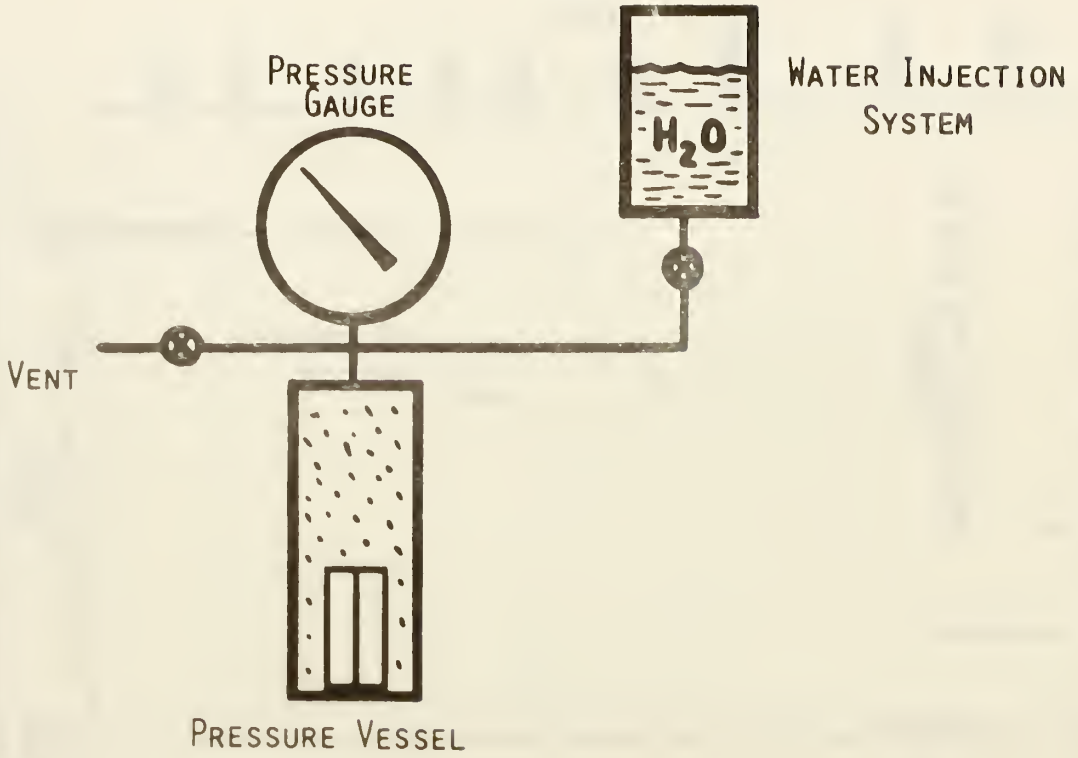

Figure 8. Schematic diagram of hydrothermal exposure equipment.

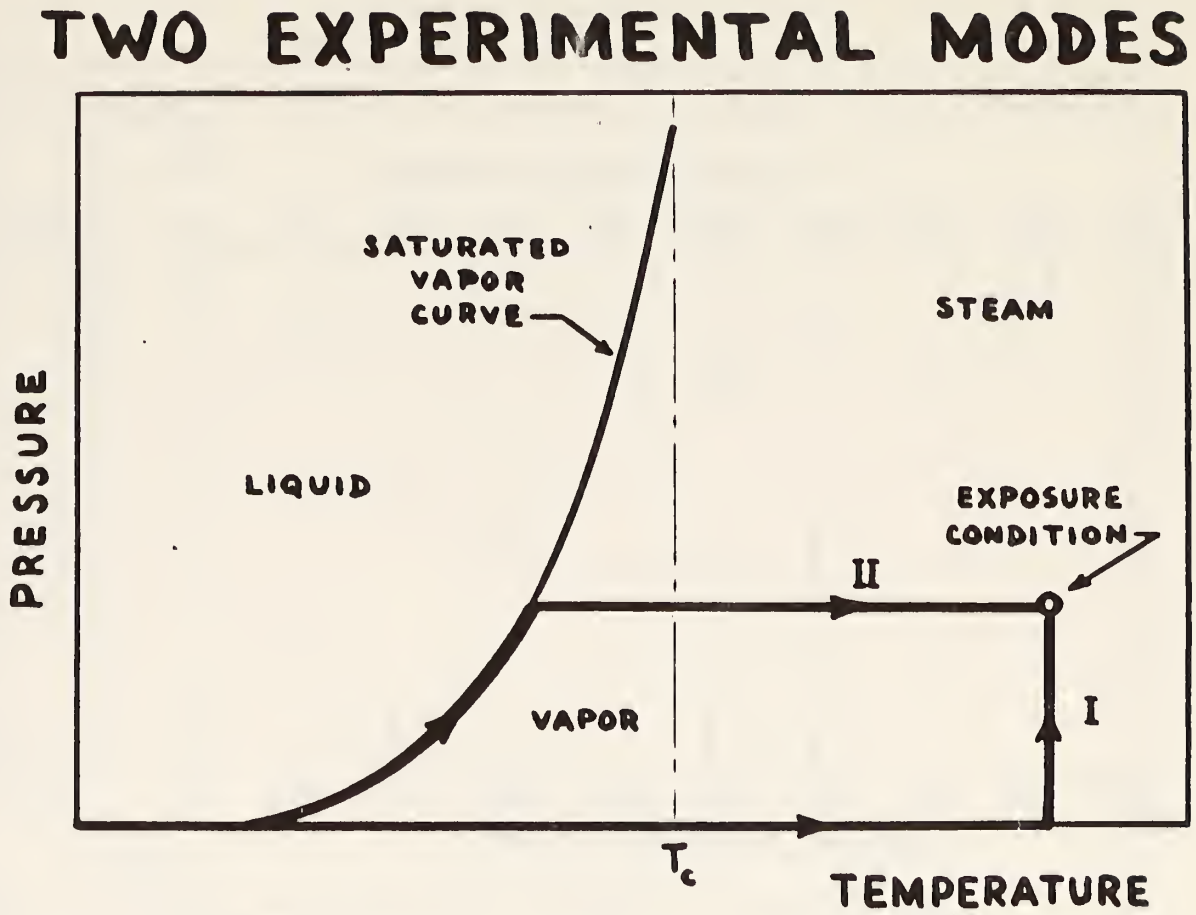

Figure 9. Schematic diagram demonstrating the two modes of operation of the hydrothermal experiment.

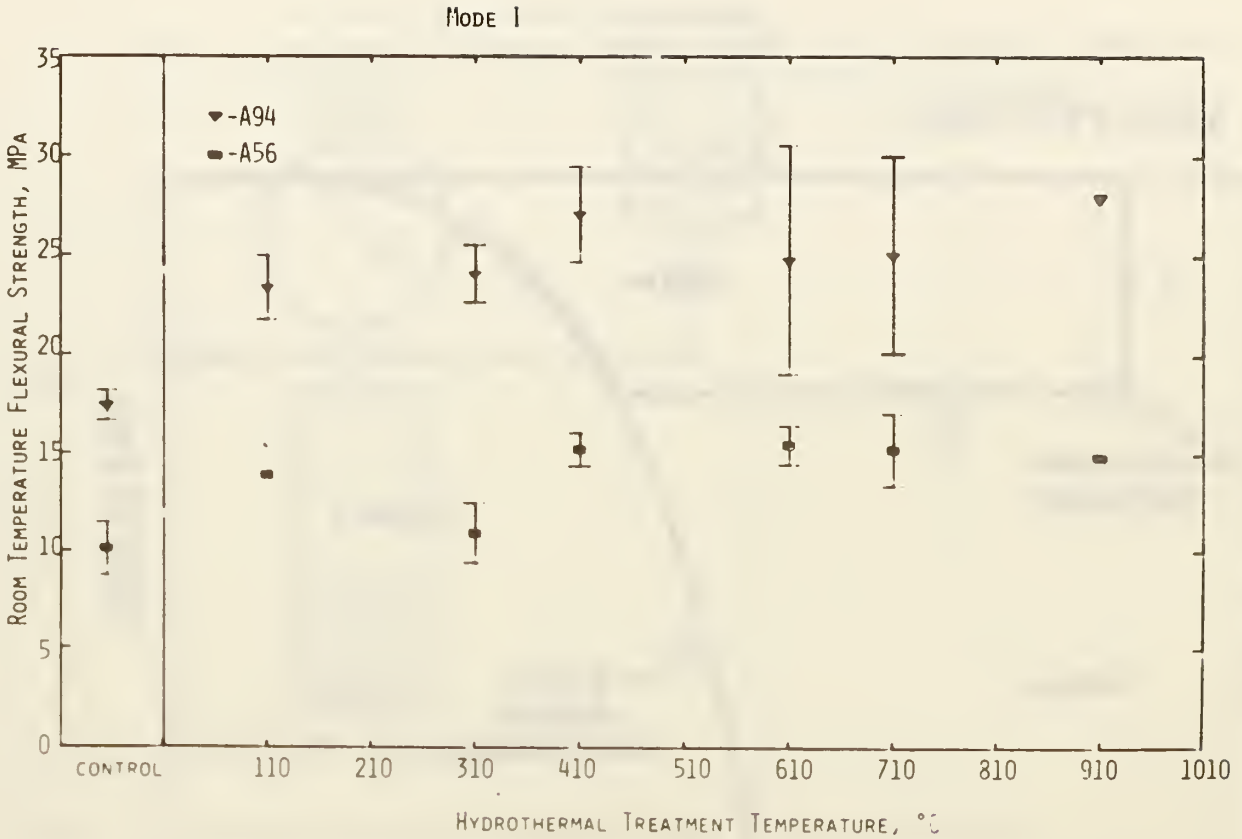

Figure 10. Effect of hydrothermal treatment on strength: Mode I operation.

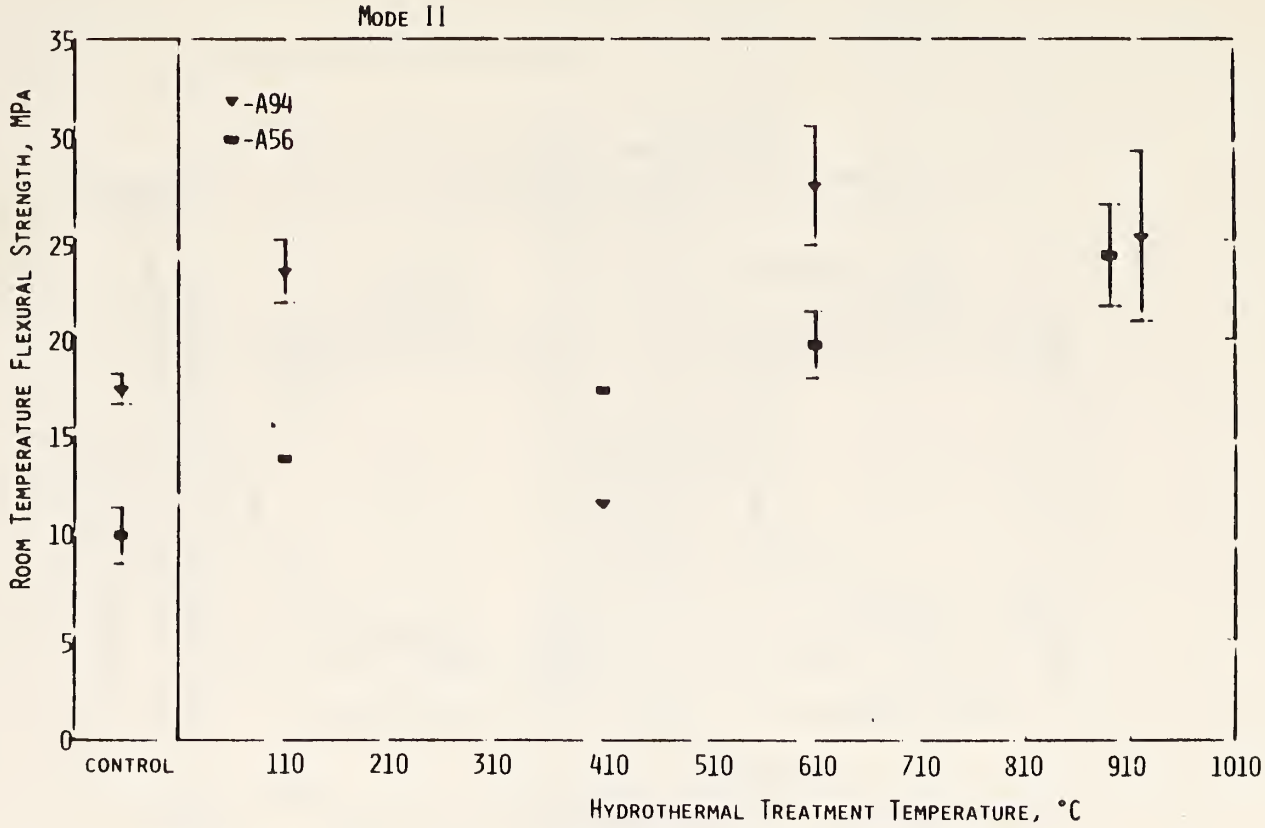

Figure 11. Effect of hydrothermal treatment on strength: Mode II operation.

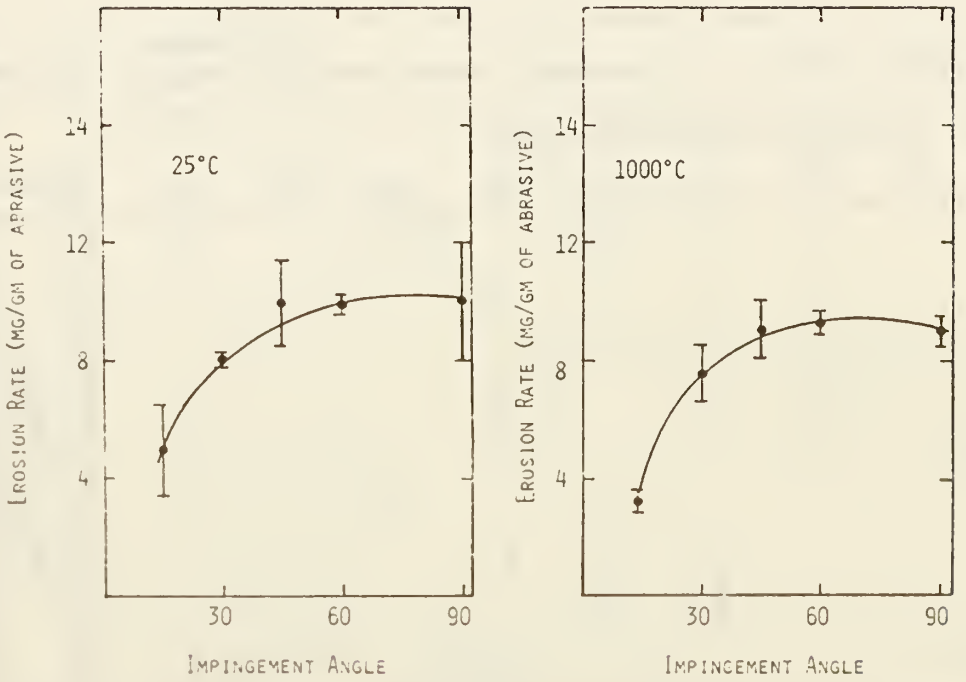

Figure 12. Effect of impingement angle on erosion rate: calcined flint clay refractory.

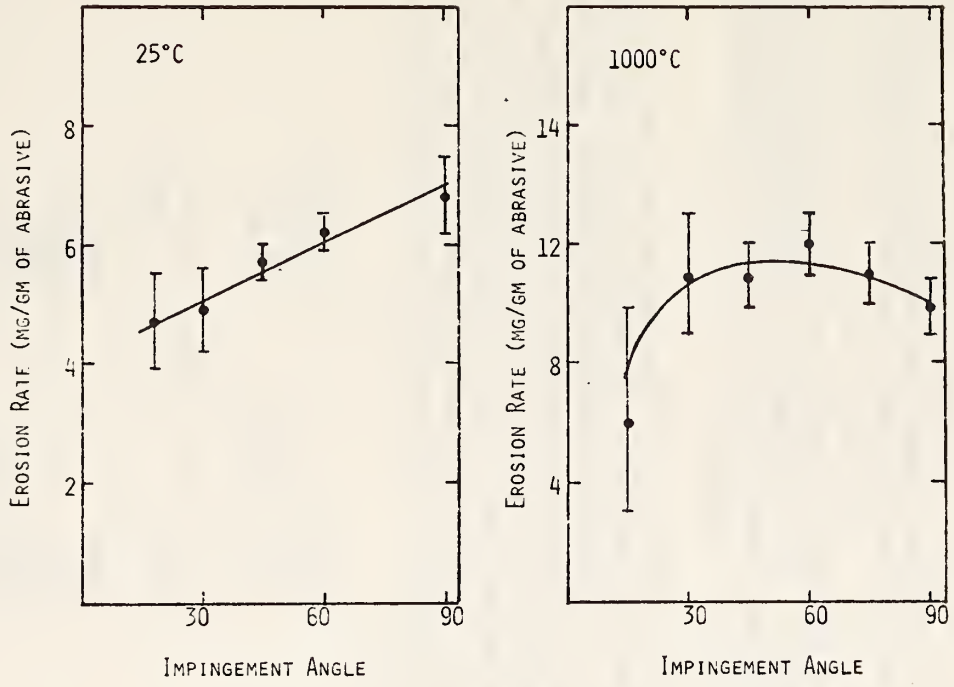

Figure 13. Effect of impingement angle on erosion rate: high purity alumina refractory.

3. Chemical Degradation of Ceramics

a. Reactions and Transformations (F. Mauer and C. R. Robbins, 313.06)

Progress: During the past quarter, work was continued on construction of the apparatus for x-ray examination of refractory castables under simulated gasification conditions. The pressure vessel and goniometer (for mounting and aligning the vessel) were completed by the NBS Instrument Shops. The specimen holder and internal heater were fabricated and installed in the pressure vessel. All components (with one exception) are now on hand and the system is ready for assembly and calibration runs. It was decided to use a new type of flange seal in the pressure vessel instead of solid copper gaskets as originally planned. Delivery of the new gaskets is expected in April.

A technician has been trained to assist in the operation of the system and in the processing of the x-ray data. A high-temperature furnace has been ordered to facilitate preparation and study of reference standards, refractories and refractory components.

The elemental analysis capability of the system was used to screen reference materials by the detection of impurities. A calculator program has been written for use in converting d-spacings and intensities of conventional powder diffraction patterns to channel numbers and counts (peaks and backgrounds) for energy dispersive diffraction (EDXD) patterns. This program was used in the interpretation of the energy dispersive patterns of reference standards shown in Figures 1 - 8. All energy dispersive patterns were recorded under the following experimental conditions:

X-ray source	Target	Tungsten
	Tube Voltage	40 kVp
	Tube current	15 mA
Diffractometer	Diffraction angle	24°(2θ)
	Slits	1°, MR,.2°
Detector	Type	Si(Li)
	Size	80mm^2
	Bias	1000V
	Resolution	225eV
Amplifier	Time constant	8μs
	Gain	8/6.0/1
	Baseline	0.04
	Polarity	Positive
Multichannel Analyzer	Conversion gain	1024
	Offset	0
	Time	300 sec(Live)
Strip chart	Vertical scale	5K/10K
	Horizontal scale	1000 chan/in.

The system was calibrated using the x-ray fluorescence lines of Ce, Zr, and Ag, in addition to the W lines of the tube spectrum. The constants a and b in the equation

$$E = a + bx$$

were obtained by linear regression for use in computing the energy, E(keV), from the channel number, x. The values obtained were a = 0.77 keV and b = 0.0354 keV per channel.

Plans: Construction of major components, and installation of specimen holder and internal heater have been completed. The system can be assembled during April and tested at high temperature. Operation will be limited to one atmosphere of pressure until the flange seals arrive. In situ x-ray diffraction measurements (Subtask 3a-3) are expected to begin in April 1977 as proposed initially.

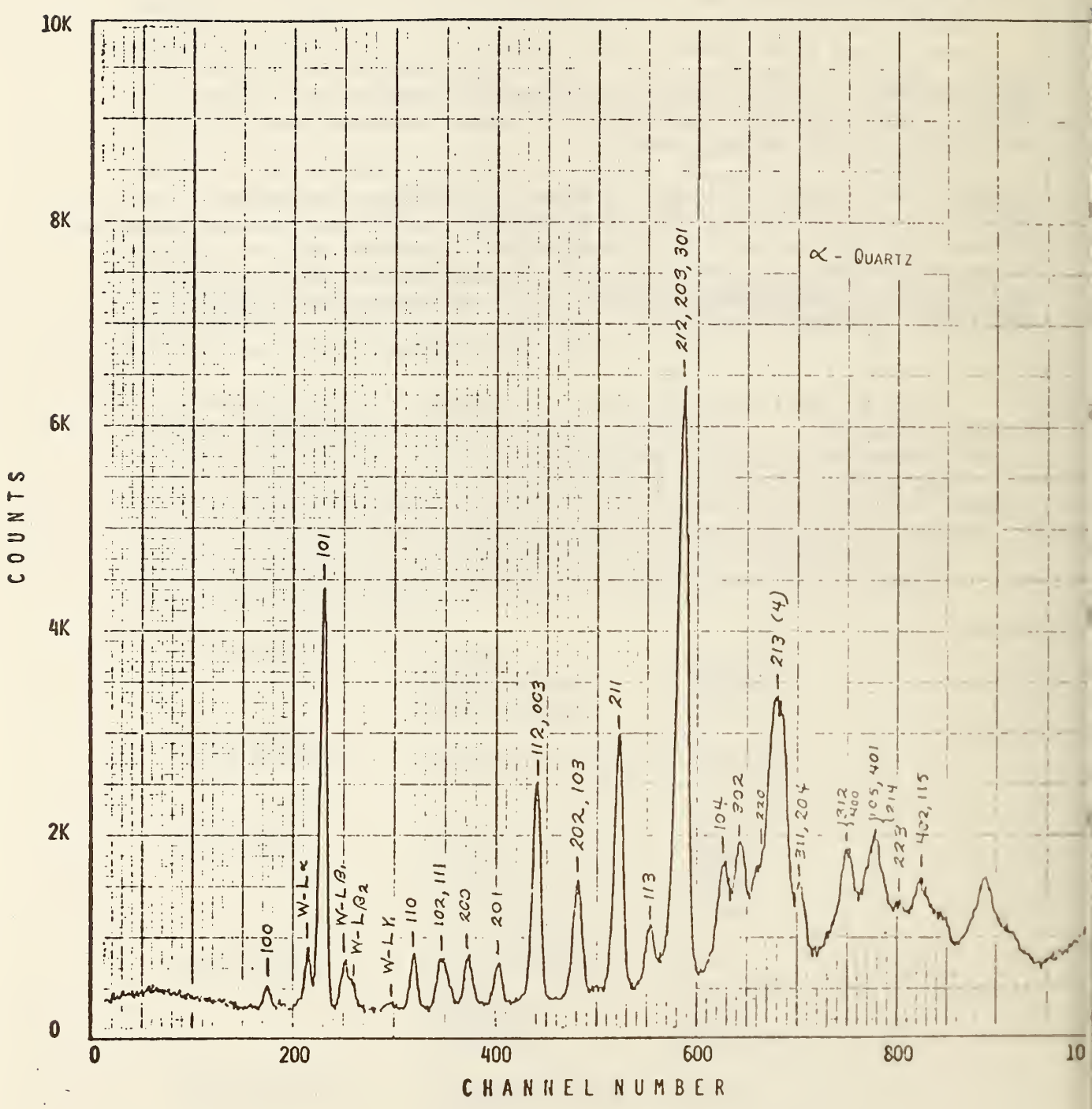

Figure 1. EDXD pattern of α-Quartz (SiO_2).

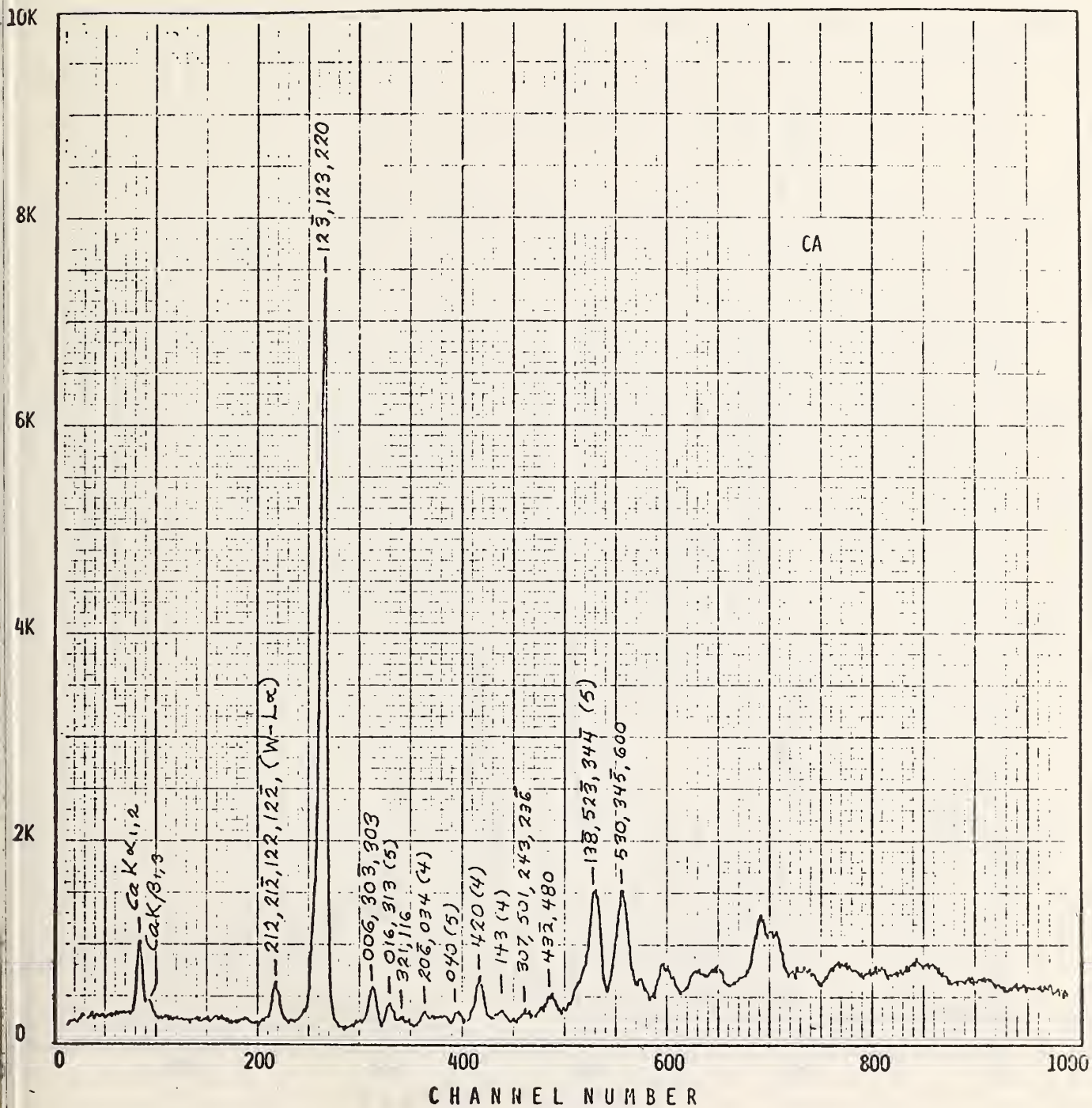

Figure 2. EDXD pattern of CA.

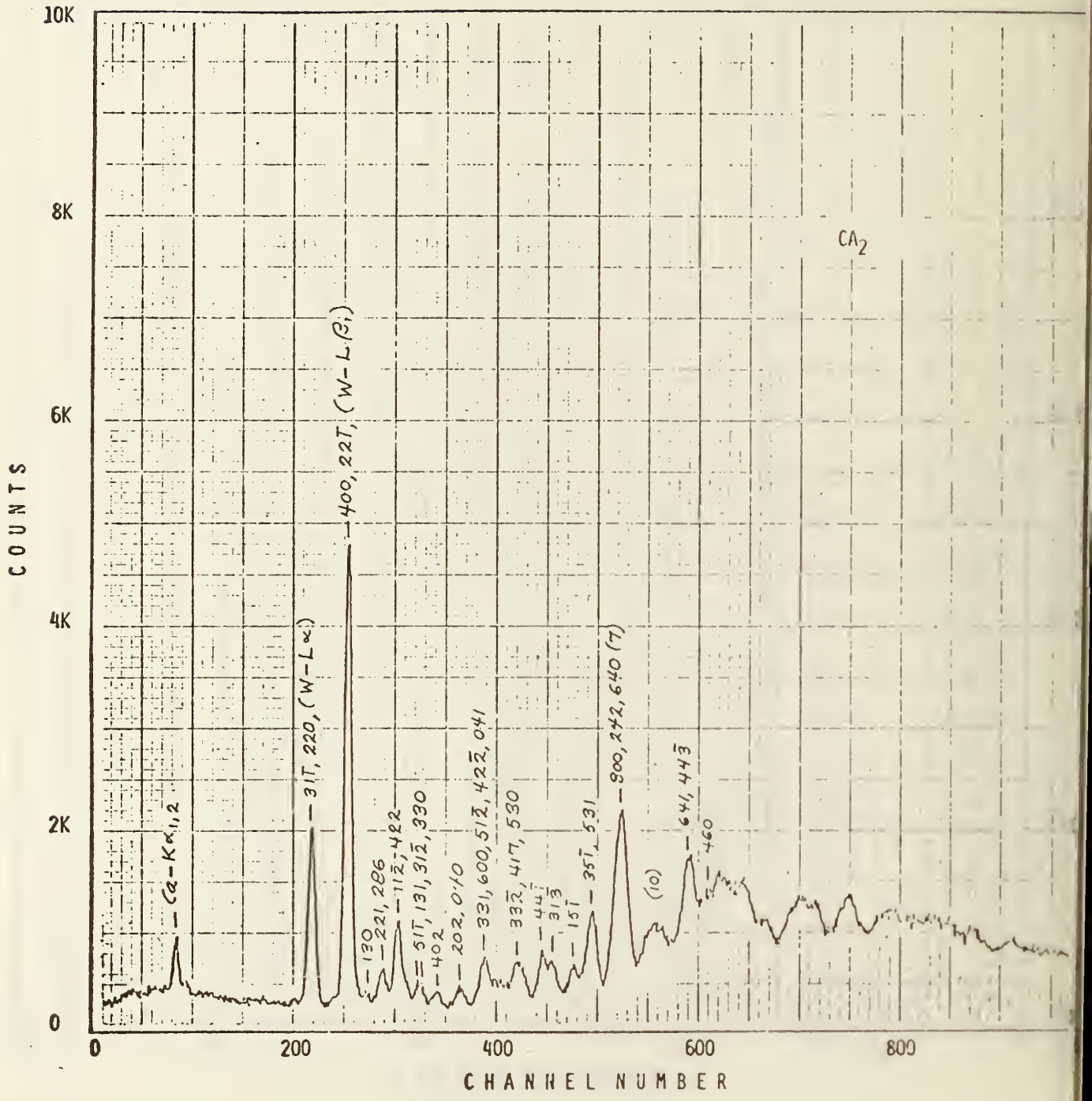

Figure 3. EDXD pattern of CA_2.

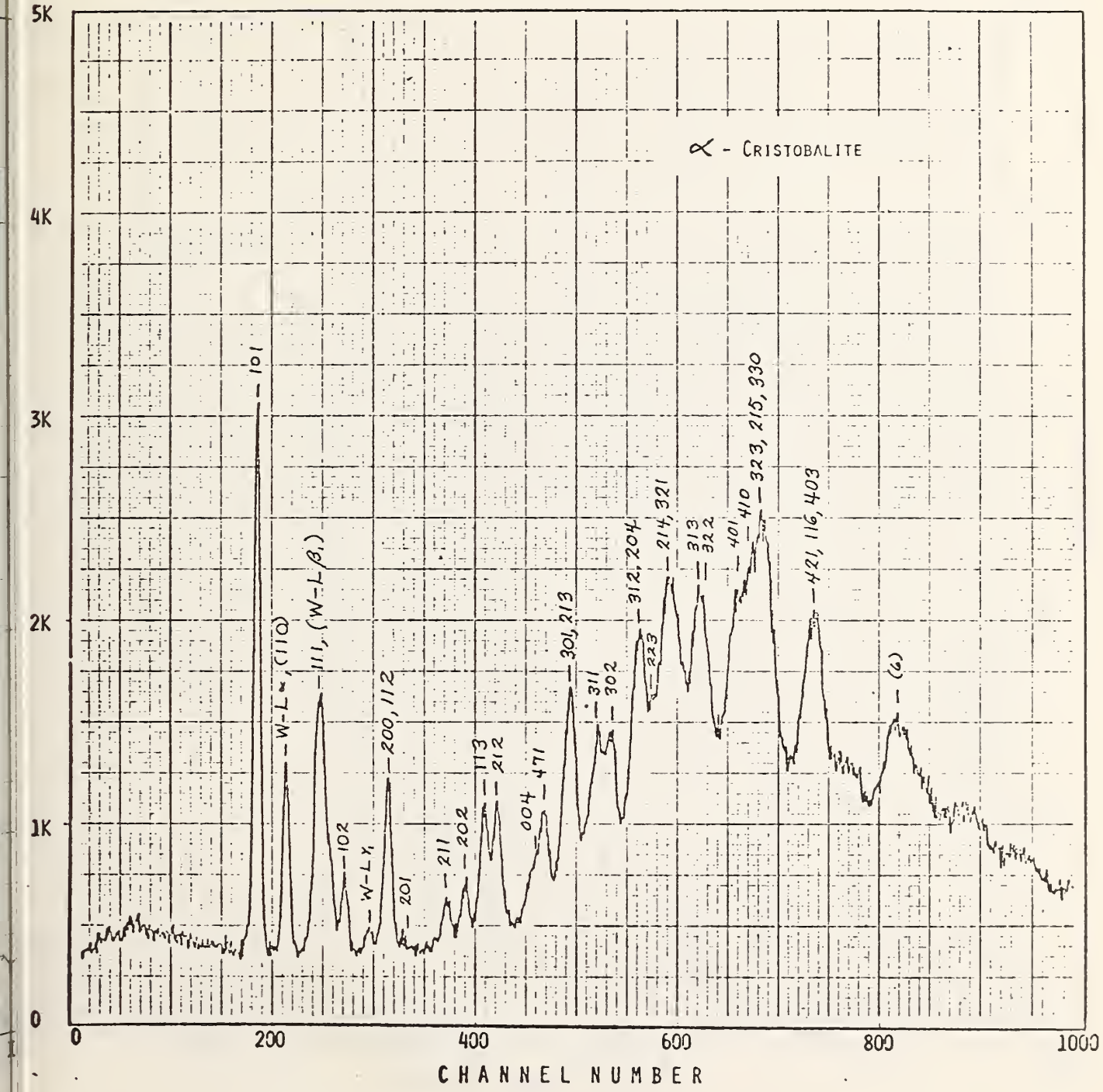

Figure 4. EDXD pattern of α-Cristobalite (SiO_2).

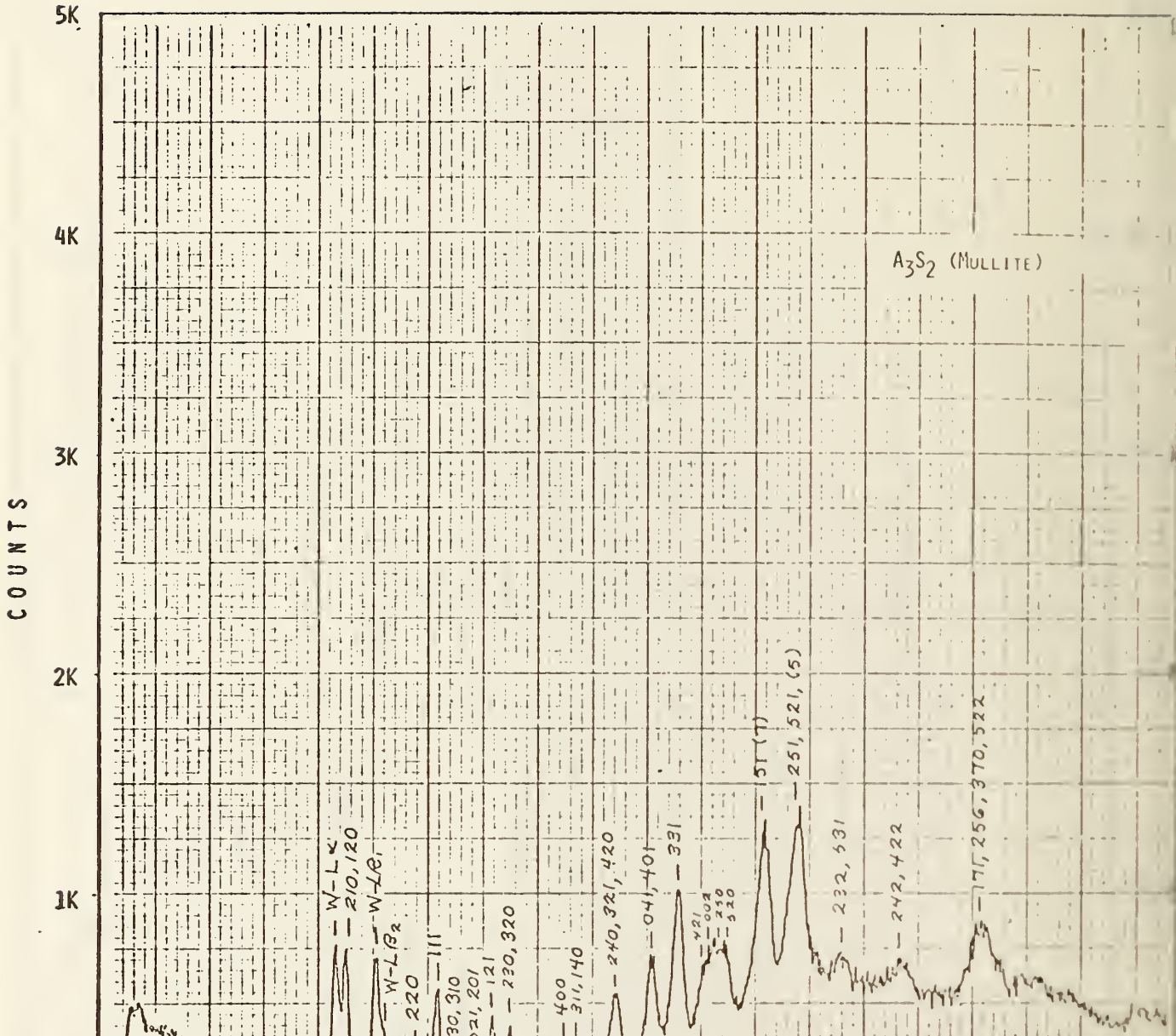

Figure 5. EDXD pattern of A_3S_2 (Mullite).

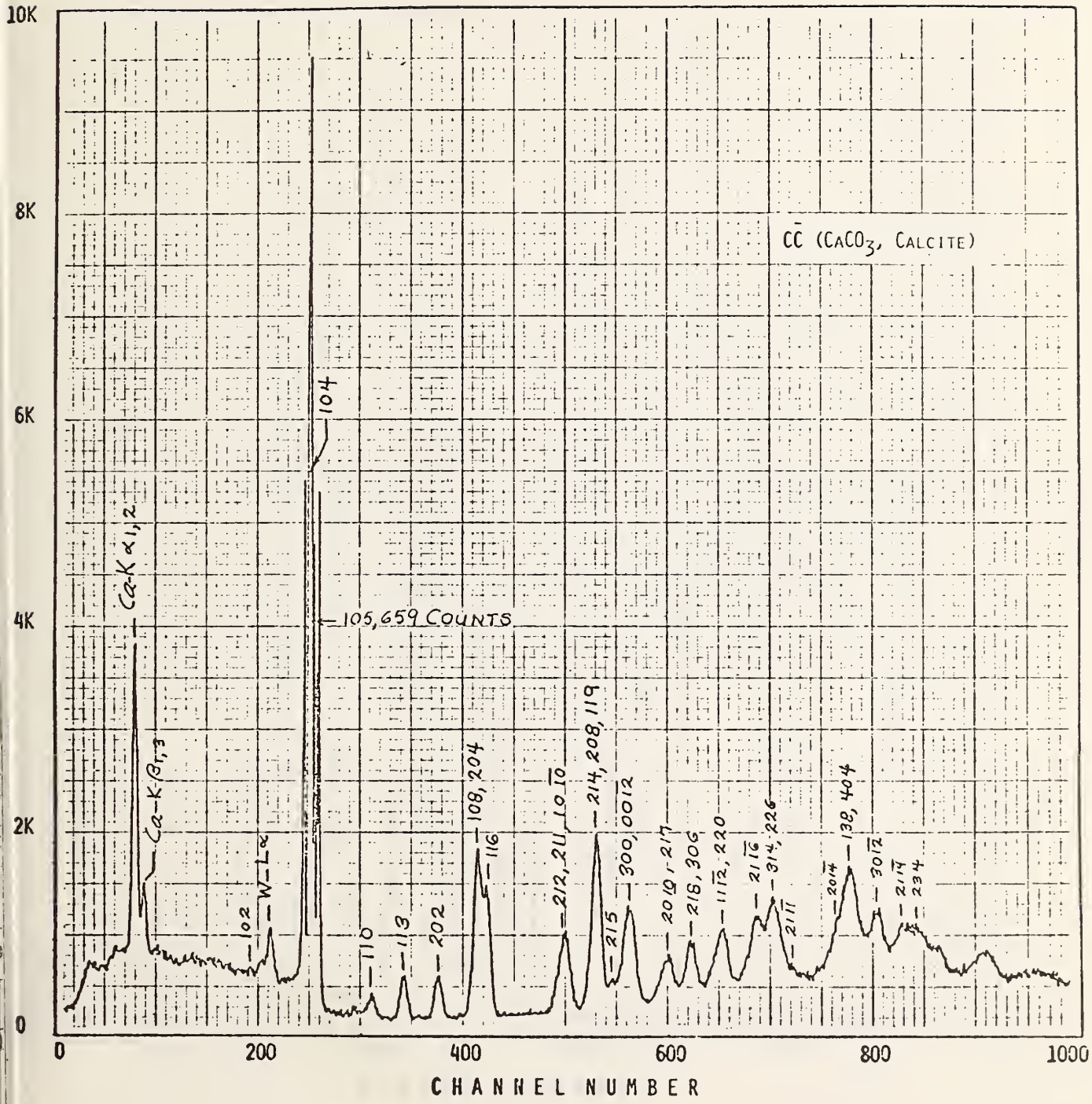

Figure 6. EDXD pattern of Calcite ($CaCO_3$).

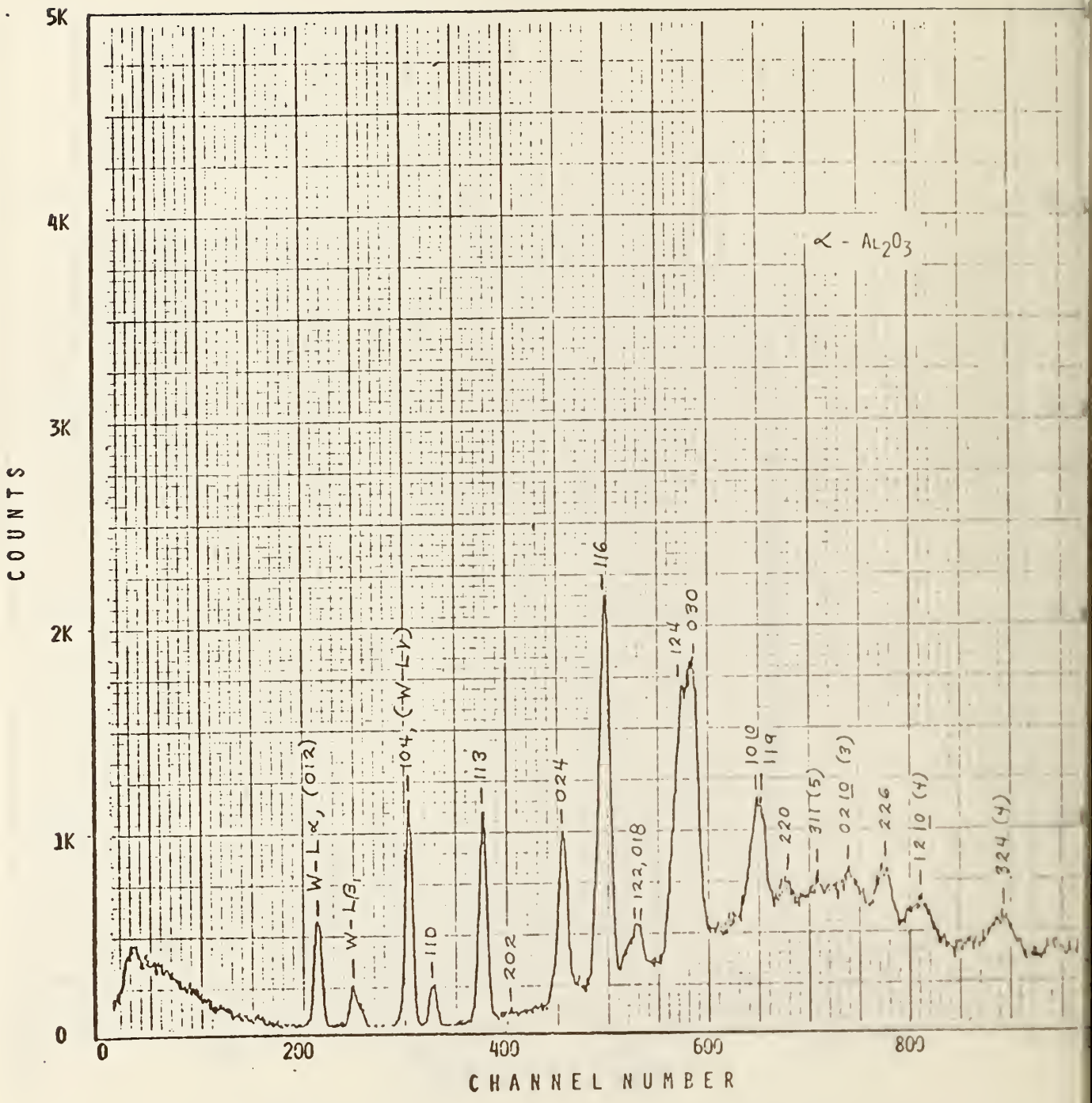

Figure 7. EDXD pattern of α-Al_2O_3.

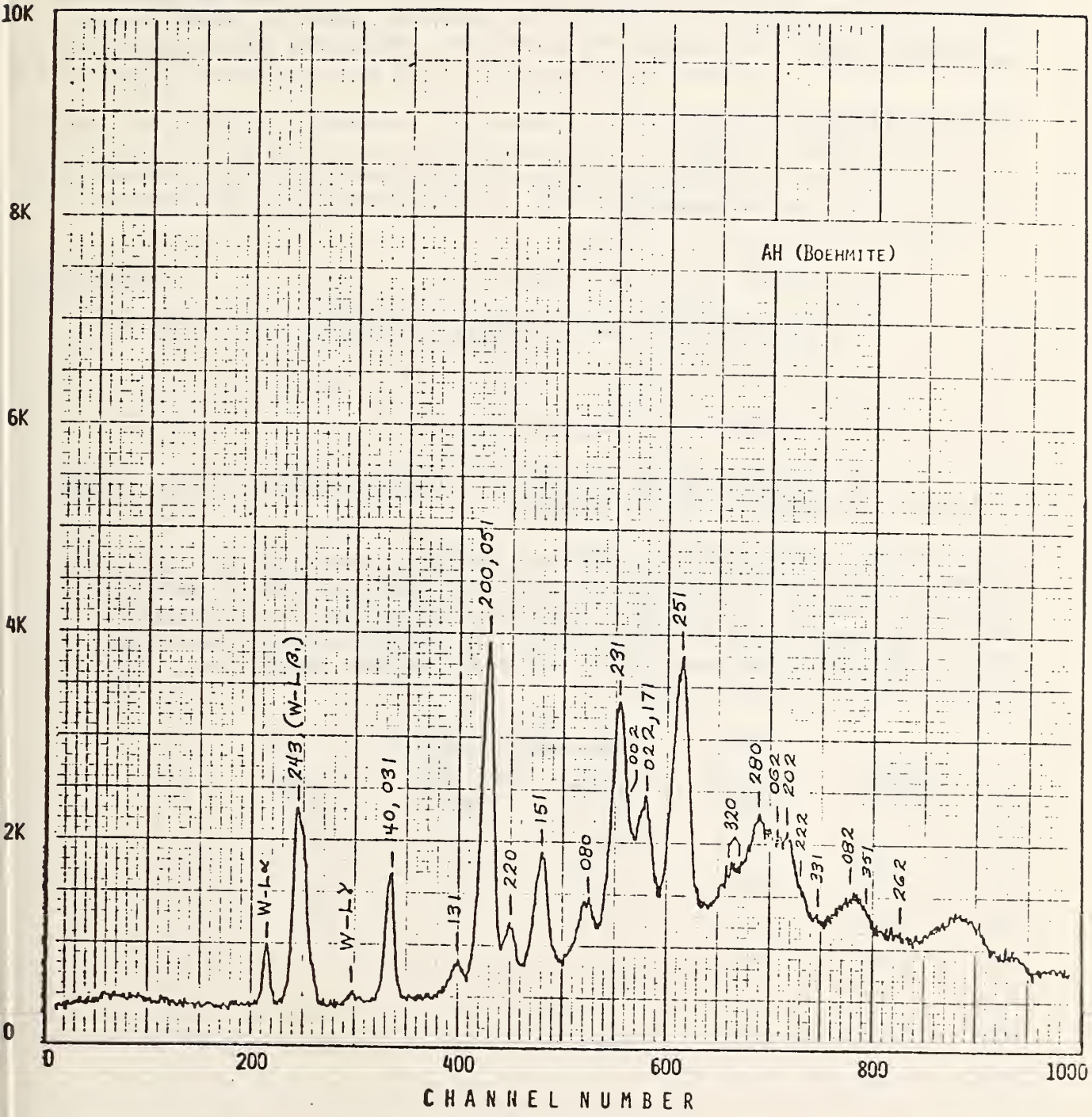

Figure 8. EDXD pattern of AH (Boehmite).

b. Slag Characterization (W. S. Brower, J. L. Waring, 313.03 and D. H. Blackburn, 313.02)

Progress: Watt and Fereday (1) measured the viscosity temperature relations of the ashes of a large number of British coals. From these measurements an equation was developed to calculate viscosity at any temperature and composition within specified limits. The important oxides in their viscosity calculations are SiO_2, Al_2O_3, Fe_2O_3, and CaO. All other oxides were grouped with MgO and ignored.

The Watt-Fereday equation is

$$\log_{10} \eta = \frac{10^7 M}{(T-150)^2} + C$$

where η is viscosity in poises

$$M = 0.00835\ (SiO_2) + 0.00601\ (Al_2O_3) - 0.0109$$

$$C = 0.0415\ (SiO_2) + 0.0192\ (Al_2O_3) + 0.0276$$

$$(\text{equivalent } Fe_2O_3) + 0.0160\ (CaO) - 3.92$$

T is temperature in degrees Celsius.

The oxides in parentheses are the concentrations of these oxides in the melt expressed in weight precents.

To determine if this equation would be useful in describing the viscosity-temperature relations for slags derived from American coals at ambient pressures a series of synthetic slags were prepared and the viscosities determined over a range of temperature. The compositions of these slags were varied about the composition of a model Montana Rosebud Ash. The compositions are given in Table 1.

Table 1. Slag Compositions wt.%

	Rosebud	No. 384	No. 352	No. 360	No. 389
SiO_2	42.10	40.0	45.0	50	30
Al_2O_3	19.50	20.0	20.0	25	30
Fe_2O_3	7.11	15.0	15.0	12	20
CaO	24.48	17.0	15.0	8	14
Na_2O	0.21				
K_2O	0.10				
MgO	5.50	8.0	5.0	5	6
TiO_2	0.90				

The viscosity of Rosebud coal ash is given in Fig. 1 together with the viscosity calculated using the Watt-Fereday equation. The measured and calculated viscosities for the other compositions in Table 1 are given in Fig. 2 and Fig. 3. The predicted viscosities seem to agree reasonably well with the measured values at ambient pressure. Measurements of viscosity will be made later on these compositions as a function of pressure of steam.

We feel that fairly satisfactory predictability is possible at ambient pressures, at least for this series of compositions, it is also reasonable that the Watt-Fereday equation can be used as a base for predicting viscosity relations as a function of steam pressure.

The pressure vessel to contain the viscosity apparatus has been constructed and pressure tested and has been delivered to the Bureau.

Plans: The torsion suspension, cup rotator, heater, and angular displacement sensor will be installed in the pressure vessel. When the internal parts of the pressure vessel have been installed, the slag compositions in Table 1 will be used for preliminary viscosity measurements at modest steam pressures.

References

1. J. D. Watt and F. Fereday, J. Inst. of Fuel, 338, 99 (1969).

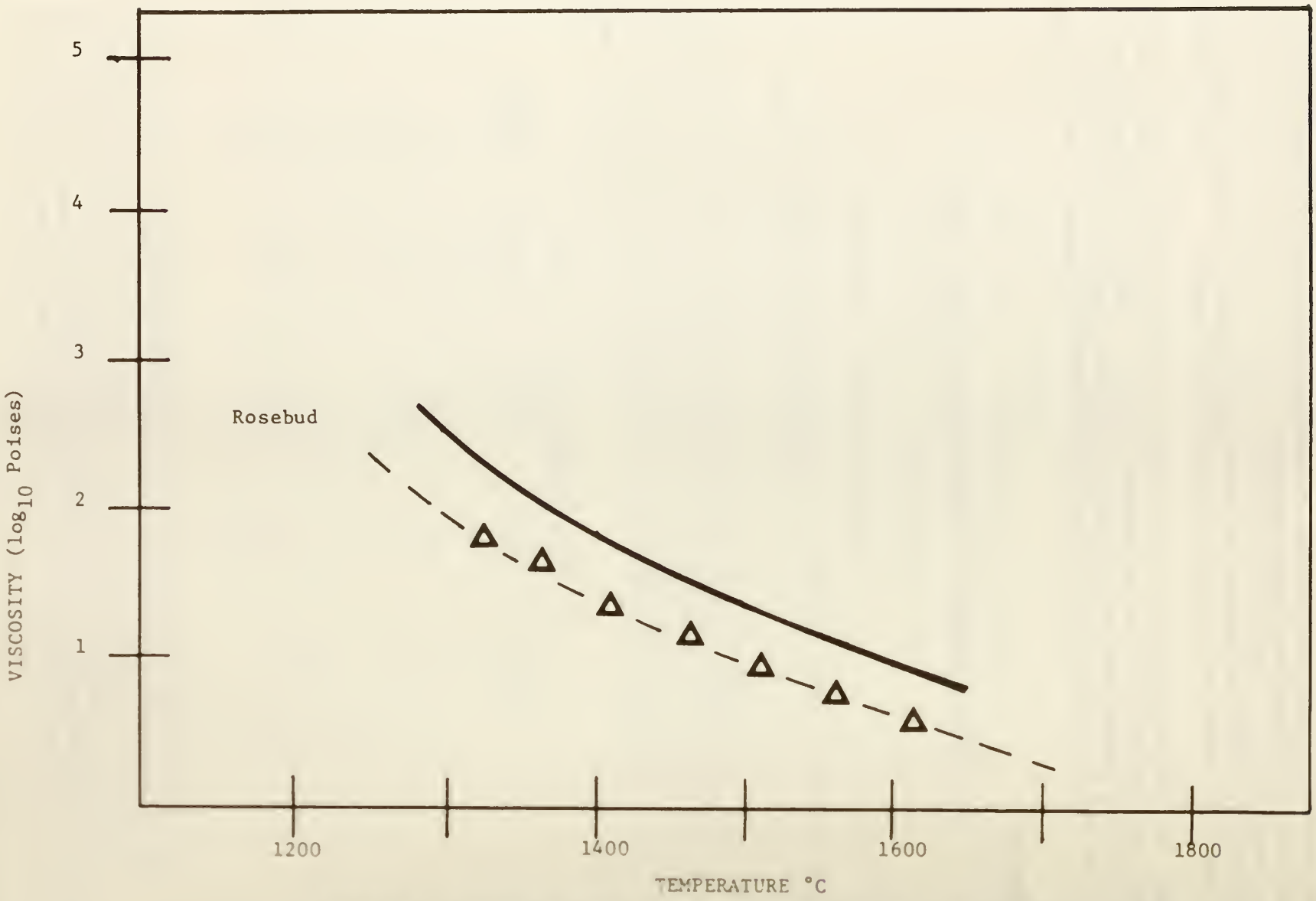

Figure 1 VISCOSITY-TEMPERATURE RELATIONSHIPS OF COAL SLAGS
Solid lines are Watt-Fereday calculated curves.

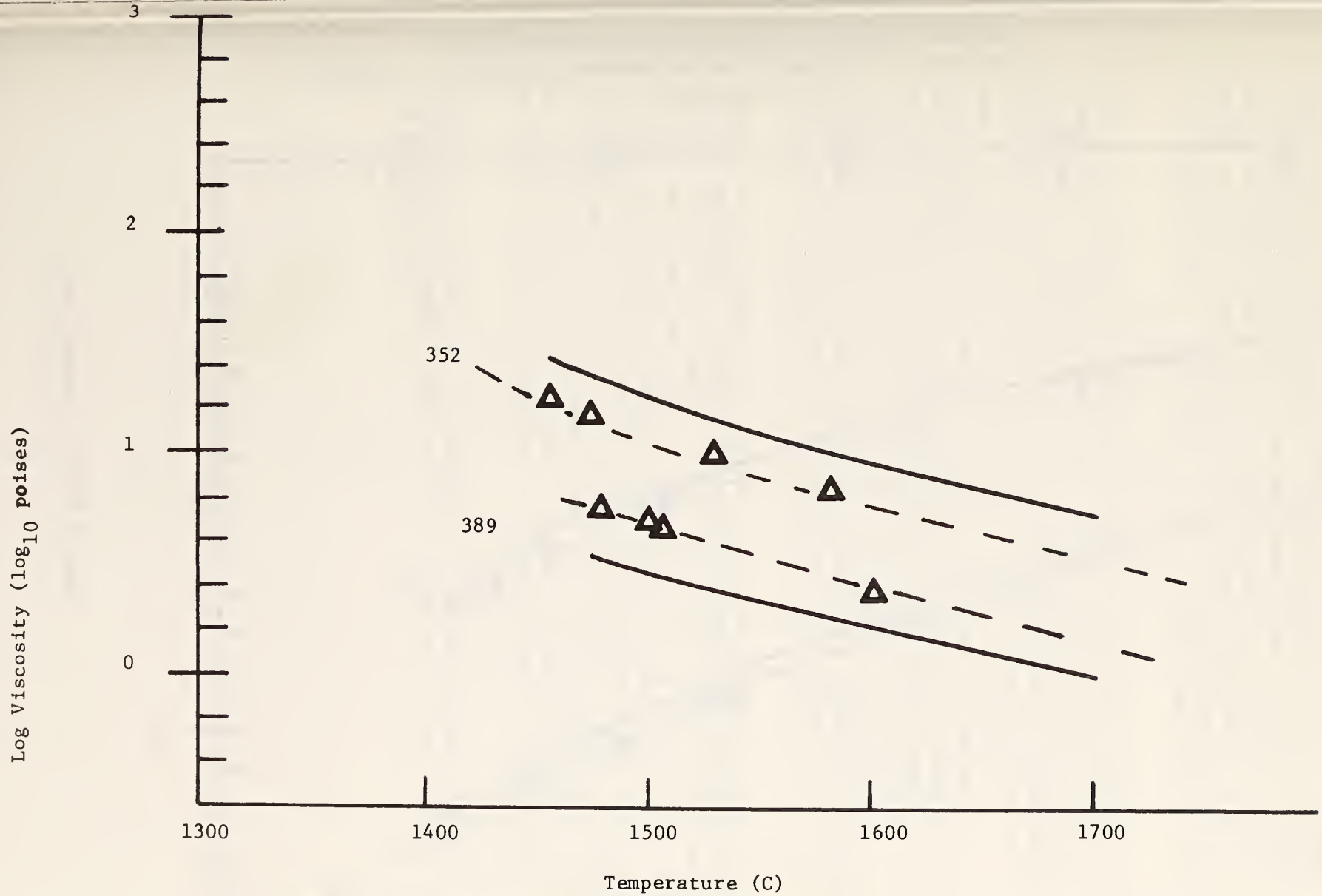

Figure 2 VISCOSITY-TEMPERATURE RELATIONSHIPS OF COAL SLAGS
Solid lines are Watt-Fereday calculated curves.

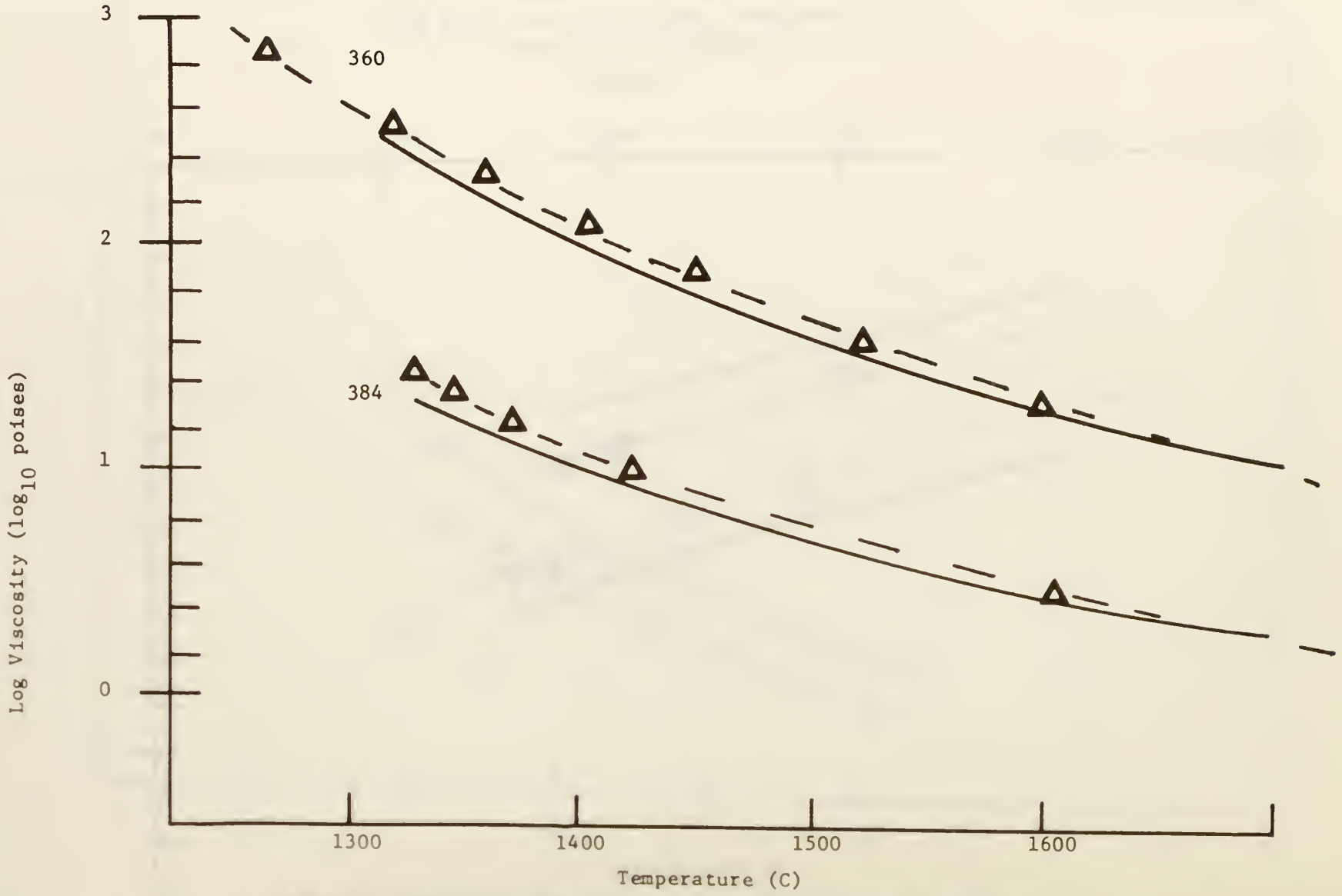

Figure 3 VISCOSITY-TEMPERATURE RELATIONSHIPS OF COAL SLAGS
Solid lines are Watt-Fereday calculated curves.

c. Vaporization and Chemical Transport (J. Hastie and D. Bonnell, 313.01)

Progress: A new reactor was constructed to allow for a new skimmer design and for water cooling at a platinum-stainless steel junction which previously failed at elevated temperatures (~1200°C). A new series of calibrations are in progress with this reactor using Na_2SO_4 as a test case. Results for this salt reported on in the previous quarterly report (Oct. 1-Dec. 31, 1976) seemed to indicate satisfactory reactor performance for the dissociative process:

$$Na_2SO_4(\ell) = 2Na + SO_2 + O_2$$

However, no $Na_2SO_4(g)$ species were observed and this is contrary to a very recent report by Kohl *et al.* (1975) from Knudsen effusion experiments. As the work of Kohl *et al.**, differed from the results of several other investigators, where $Na_2SO_4(g)$ was not observed, we repeated the Kohl *et al.*, experiments using our Knudsen effusion mass spectrometer system. Our results showed the presence of Na_2SO_4 together with Na, SO_2, and O_2, under what are believed to be thermodynamic equilibrium conditions. Hence the presence of Na_2SO_4 in the high pressure transpiration-type reactor should be a good indication of gas saturation and overall thermodynamic equilibrium in the reactor. A preliminary test with the newly constructed reactor has verified the presence of $Na_2SO_4(g)$, as expected for an equilibrium system, over liquid Na_2SO_4 at temperatures and total pressures of 1300-1700 K and 290-620 Torr respectively.

Plans: Following completion of the first phase of calibrations and tests for the new reactor, using the simple salts Na_2SO_4 and NaCl, a second phase of tests will be made. This will involve more complex chemical systems where reactive coal gas components such as H_2O, H_2, SO_2, and HCl will be allowed to interact with Na_2SO_4 (initially). As the thermodynamics of above mentioned species are known, then the reaction products can be predicted and an assessment made of whether equilibrium occurs under our reaction conditions. A new gas handling system will be constructed for these studies. We plan to present a paper on our new mass spectrometric technique at the next annual meeting of the American Society for Mass Spectrometry (Washington, D.C., May 1977).

*Kohl, J.F., Stearns, A. C. Fryburg, C. G., "Sodium Sulfate: Vaporization Thermodynamics and Role in Corrosive Flames," NASA TM X-71641 (1975).

4. Failure Prevention (J. H. Smith and W. A. Willard, 312.01)

Progress: During this quarter the Failure Prevention Information Center received approximately 40 reports of operational malfunctions and component failures in coal conversion pilot plants and process development units. These reports included several diagnostic failure analysis reports from Argonne National Laboratories and Oak Ridge National Laboratories.

These reports have been classified and evaluated for technical completeness and accuracy. Detailed abstracts of this information have been entered into the CCA Model 204 computerized data base management system for ease of future retrieval and data dissemination. An update of the frequency of failure modes which analyzes the information contained in the system is shown in Table 1.

The Information Center has collaborated closely with Battelle-Columbus in the preparation of the ERDA Materials and Components Newsletter. Weekly updates of all abstracts are furnished to Battelle along with complete copies of all significant information. During this quarter, 21 separate requests for information have been received by the Information Center. In response to these inquiries, copies of 400 abstracts, 26 complete information items, and 48 print-outs of statistical programs were sent out.

Five visitors who were interested in the Center's operation were briefed on the method of operation and types of output the computerized system is able to produce.

Five draft reports to be used for efficiently disseminating information from the Failure Prevention Information Center were prepared. These reports cover operating discrepancies and component failures from the CO_2, HYGAS, SRC and Synthane Pilot Plants. The other report covers the use of Incoloy 800 in several components and the various failure modes to which this alloy is susceptible.

Various statistical programs have been developed for use with the data base management system. These programs are now complete and in use. They enable the Center to perform statistical analyses on failure mode, type of component, materials of construction, and coal conversion processes. See Tables 2 and 3 for examples of these programs.

Plans: The information collecting phase of this task will continue as more information is received on a continuing basis from the pilot plants. Visits to operating pilot plants and failure analysis laboratories are planned to significantly augment the information collection activities and to get additional information on operating discrepancies and component failures. The abstract reports that have been prepared will be thoroughly reviewed, corrections made and issued.

Table 1

3/30/77

FREQUENCY OF FAILURE MODE

Cause of Incident	No. of Items	CO_2	HYGAS	SRC	Synthane	Others
Corrosion	129					
Carburization	12	7	3	0	0	2
General	62	3	7	8	12	32
Metal Dusting	5	3	0	0	0	2
Oxidation	8	4	3	0	0	1
Pitting	12	3	2	2	1	4
Sulfidation	30	14	10	0	6	0
Design Defect	48					
General	43	6	3	12	5	17
Thermal Stresses	5	0	2	1	0	2
Erosion	64	8	6	10	16	24
Fabrication	15	4	4	0	4	3
Welding	10	2	3	0	2	3
Quality Control	18	4	3	0	6	5
SCC-CL	31	4	4	2	4	17
Undetermined	32	2	11	0	13	6

Table 2

COAL CONVERSION PROCESSES

NO OF ITEMS	PERCENT	PROCESS
7	1.96	ALL
1	0.28	BIGAS
14	3.93	BMI
10	2.80	CARBONATE
13	3.65	CLEAN COKE
1	0.28	COED
70	19.66	CO2
1	0.28	CPC
64	17.97	HYGAS
1	0.28	LERC
24	6.74	LIGNITE
2	0.56	MERC
26	7.30	MISC.
2	0.56	PERC
1	0.28	RANN
2	0.56	SEVERAL
30	8.42	SRC
1	0.28	SRC-W
69	19.38	SYNTHANE
2	0.56	SYNTHOIL
1	0.28	UNKNOWN
14	3.93	WESTINGHOUSE

356 = TOTAL NUMBER OF ITEMS IN FILE

Table 3

COMPONENT FAILURES-ALL PROCESSES

NO OF ITEMS	COMPONENT
44	AUXILIARY PROCESS EQUIPMENT
7	INSTRUMENTATION
42	MATERIAL EVALUATION
166	PIPING
32	BELLOWS
15	THERMOWELLS
23	PRESSURE VESSEL
5	GASIFIER
5	REGENERATOR
4	BOILER
27	PUMPS
6	ROTATING EQUIPMENT
22	THERMOCOUPLE
0	UNKNOWN
38	VALVES

U.S. DEPT. OF COMM. BIBLIOGRAPHIC DATA SHEET	FE-3800-11 NBSIR 77-1252	No.	

4. TITLE AND SUBTITLE

"MATERIALS RESEARCH FOR CLEAN UTILIZATION OF COAL"
Quarterly Progress Report, January 1 - March 31, 1977

5. Publication Date: April 1977

6. Performing Organization C: NBSIR 77-1252

7. AUTHOR(S): Samuel J. Schneider, Jr.

8. Performing Organ. Report

9. PERFORMING ORGANIZATION NAME AND ADDRESS

NATIONAL BUREAU OF STANDARDS
DEPARTMENT OF COMMERCE
WASHINGTON, D.C. 20234

10. Project/Task/Work Unit N

11. Contract/Grant No.: E(49-1)-3800

12. Sponsoring Organization Name and Complete Address (Street, City, State, ZIP)

Energy Research and Development Administration
20 Massachusetts Avenue
Washington, D. C. 20545

13. Type of Report & Period Covered: Quarterly Progress Report

14. Sponsoring Agency Code: Dist. Cat. UC-90

15. SUPPLEMENTARY NOTES

16. ABSTRACT (A 200-word or less factual summary of most significant information. If document includes a significant bibliography or literature survey, mention it here.)

This progress report covers work on metal corrosion, metal erosion, ceramic deformation, fracture, erosion, and chemical degradation as related to coal gasification systems. This report also covers the failure avoidance program for ERDA coal conversion pilot plants.

17. KEY WORDS (six to twelve entries; alphabetical order; capitalize only the first letter of the first key word unless a proper name; separated by semicolons) Ceramic corrosion, cermaic erosion, ceramic fracture, che degradation, coal gasification material, failure avoidance, metal corrosion, meta erosion, vaporization processes

18. AVAILABILITY

☐ Unlimited

XX For Official Distribution. Do Not Release to NTIS NBS will not submit to NTIS; ERDA-FE will submit after approval.

☐ Order From Sup. of Doc., U.S. Government Printing Office Washington, D.C. 20402, SD Cat. No. C13

☐ Order From National Technical Information Service (NTIS) Springfield, Virginia 22151

19. SECURITY CLASS (THIS REPORT): UNCLASSIFIED

21. NO. OF P: 69

20. SECURITY CLASS (THIS PAGE): UNCLASSIFIED

22. Price

USCOMM-DC